Sara Stoppacher, BSc

External stimulation of excitable heart and brain cells

Master's Thesis

to achieve the university degree of

Diplom-Ingenieurin

Master's degree programme: Biomedical Engineering

submitted to

Graz University of Technology

Supervisor

Rienmüller, Theresa Margarethe, Ass.Prof. Dipl.-Ing. Dr.techn.

Institute for Health Care Engineering
Head: Baumgartner, Christian, Univ.-Prof. Dipl.-Ing. Dr.techn.

Graz, December 2019

Affidavit

I declare that I have authored this thesis independently, that I have not used other than the declared sources/resources, and that I have explicitly indicated all material which has been quoted either literally or by content from the sources used. The text document uploaded to TUGRAZonline is identical to the present master's thesis.

_____   _____
            Date   Signature

Abstract

The aim of this work was to find out whether it is possible to stimulate excitable cells via external stimulation and to trigger an action potential using a novel technology called Photocap. Photocaps are light-sensitive organic photocapacitors. The key question of this work was answered by implementing a proper simulation model. Therefore, it was necessary to carry out a comprehensive characterization of this novel device. In the end the maximum voltage generated by a Photocap was sent to a virtual cell in an implemented mixed model of Luo-Rudy and Ebihara-Johnson. It was demonstrated that it is possible to trigger action potentials of excitable cells through a Photocap.

5 key words: Photocap, external stimulation, equivalent circuit, cell model, simulation

Ziel dieser Arbeit war, herauszufinden ob erregbare Zellen durch externe Stimulation mithilfe einer neuartigen Technologie namens Photocap getriggert und ein Aktionspotenzial auslösen können. Ein Photocap ist ein lichtempfindlicher organischer Photokondensator. Die Kernfrage dieser Arbeit sollte durch Implementierung eines geeigneten Simulationsmodells beantwortet werden. Im Zuge dieser Arbeit wurde eine umfassende Charakterisierung von Photocaps durchgeführt, welche schlussendlich die Parameter für das Simulationsmodell lieferten. Die maximal erzeugbare Spannung eines Photocaps wurde abschließend in ein implementiertes Mischmodell von Luo-Rudy und Ebihara-Johnson an eine virtuelle Zelle geschickt. Am Ende dieser Arbeit wurde gezeigt, dass es möglich ist Aktionspotenziale erregbarer Zellen durch ein Photocap auszulösen.

5 Schlüsselwörter: Photocap, externe Stimulation, äquivalente Schaltung, Zellmodell, Simulation

Acknowledgments

I would like to take this opportunity to thank everyone who has supported me not only during the preparation of my master thesis, but especially during my entire study period.

First of all, I would like to thank Prof. Theresa Rienmüller, who has supervised my master thesis. She has always supported me with great tips and assistance. I appreciate her commitment and her constructive criticism. Thank you very much!

Furthermore, I would like to thank the entire team of the HCE Institute for their constant support and the opportunity to participate in this exciting project, especially Prof. Christian Baumgartner.

My very special and deepest thanks go to my whole family, especially to my parents Ursula and Christian. Both of them have taught me to approach new situations open-heartedly and optimistically and to accept new challenges. In case of failure I could always count on their support, motivating and constructive words and open arms. Thank you for everything!

I would also like to thank my uncle Rupi for inspiring me for technology from childhood on. His never-ending ideas in technical matters have inspired me to start my own journey in the search of technological innovations.

Last but not least, I would like to thank my boyfriend Lucas for always standing by my side, always having an open ear and supporting me in all my projects. I really appreciate that I have not only found the love of my life in him, but also someone with whom I like to discuss things and dream together.

List of abbreviation

acc	according
AP	Action potential
approx.	approximately
BR	Beeler Reuter
e.g.	for example
EIS	Electrical Impedance Spectroscopy
EJ	Ebihara Johnson
EPR	Electrical PhotoResponse
eq.	Equation
etc	meaning "and the rest"
fig.	Figure
FM	free membrane
FP	Field Potential
HH	Hodgkin Huxley
iHCE	Institute of Health Care Engineering
JM	junction membrane / attached membrane
LR	Luo Rudy
LREJ	Luo Rudy Ebihara Johnson model
PN	A material transition in semiconductor crystals
SD	Strength-duration
TBI	Traumatic Brain Injury
TDS	Two domain system
vs.	versus

Contents

Contents

List of Figures

List of Figures

List of Figures

1. Introduction

Apart from physiotherapy, there exists still no long-lasting therapeutic possibility to restore the regeneration of TBI functional deficits. So-called light-activated Photocaps provide neuronal cell stimulation and should eventually lead to neuronal cell regeneration and TBI protection. A newly implemented model will be used to find out whether stimulation of excitable cells through Photocaps is possible in practice. Therefore a comprehensive basic research had to be carried out before. This chapter mainly deals with basic electrophysiological understanding, external stimulation and the structure of Photocaps. These three comprehensive topics build up a solid basic knowledge, which is necessary to understand this subject. Therefore the sources [23] and [22] were used for an entry in the basic topics.

1.1. Electrophysiological basics

Electrophysiology essentially describes the electrochemical signal transmission of excitable cells. In this chapter the electrophysiological basics are described which are essential to understand the course of this work, means the basic processes of an action potential and the first theoretical model theories of cell models are discussed and explained.

1.1.1. Action potential

The temporal course of an action potential can be divided into different phases. The electrophysiological process that happens in the background is based on the Hodgkin-Huxley theory. In the studies by Hodgkin and Huxley, the results for the transmembrane potential were based on the Goldman-Hodgkin-Katz equation (GHK), see eq. 1.1, where P_x is the permeability of the xth ion channel, where x stands for the different types of ion channels.

$$V_m = \frac{RT}{F} \ln \left(\frac{P_K[K]_e + P_{Na}[Na]_e + P_{Cl}[Cl]_i}{P_K[K]_i + P_{Na}[Na]_i + P_{Cl}[Cl]_e} \right) \qquad (1.1)$$

Nernst Potential: In equilibrium-state there is no net force in each direction. The net flux across the membrane is zero. The membrane in equilibrium-state looks as follows:

$$V_m = \frac{RT}{ZF} \ln \left(\frac{[ion]_o}{[ion]_i} \right) \qquad (1.2)$$

At the beginning, the cell is at rest and has a resting membrane potential, which is slightly higher than the potassium equilibrium potential (the so-called Nernst potential based on 1.2, for K+ shown in eq.1.3). The sodium channels are almost closed, only certain potassium channels are open. It follows that the potassium ions determine the resting membrane potential. The membrane potential at rest then looks like:

$$V_m \approx E_K = \frac{RT}{F} \ln \left(\frac{[K]_e}{[K]_i} \right) \qquad (1.3)$$

A distinction is made between two types of action potentials, the action potential of nerve cells and the one for cardiac cells. The main difference between these two species are their duration (nerve cells: about 2 ms, heart cells: about 200 ms to 400 ms) and their opening/closing mechanisms of different ion channels. In addition, the action potential of a heart cell has a plateau phase, which is based on the influx of Ca2+ ions. The different types of action potentials are shown in fig. 1.1 and fig.1.2.
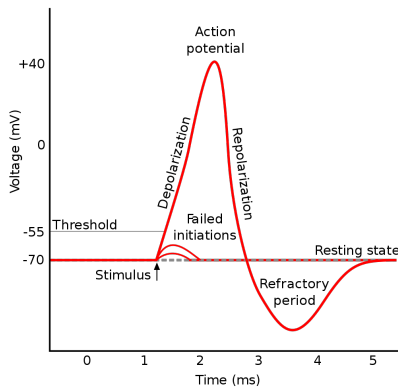
Figure 1.1.: Course of an action potential of a nerve cell [28]
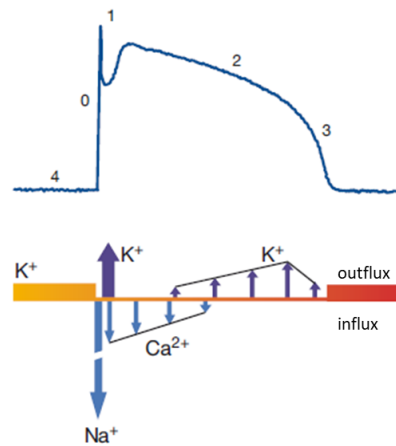
Figure 1.2.: Course of the action potential of a heart cell, modified from [10]

The following section describes the individual significant phases of action potential courses:

Depolarisation: If polarisation exceeds the threshold potential, the Na+ inflow exceeds the K+ outflow. The membrane potential depolarizes and approaches the Nernst potential for Na+, but doesn't exceed it. The membrane potential at the peak then looks like:

$$V_m \approx E_{Na} = \frac{RT}{F} \ln \left(\frac{[Na]_e}{[Na]_i} \right) \tag{1.4}$$

Repolarization: Na+ channels begin to inactivate even before the potential maximum is reached. First, repolarization occurs due to the spontaneous inactivation of the Na+ conductivity, followed by accelerated repolarization due to delayed activation of the K+ conductivity (K+ outflux).

Hyperpolarization: It occurs as a result of the still increased potassium conductivity. In this phase, the potential converges even closer to the Nernst potential for K+. The K+ conductivity is increased because special potassium channels are open, due to calcium ions flowing in during the action potential.

Refractory period: After the action potential has decayed, a cell cannot be excited for a short time. In the myocardial cells of the heart, this phase - called "plateau

phase" - lasts for a long time, which is attributed to a "slow calcium influx". This circumstance is important because it prevents a reentry of the excitation.

Summarized it can be said:

- Depolarization = Na+ activation
- Repolarisation (above Zero-Axis) = Na+ inactivation
- Accelerated repolarization (below Zero-Axis) = K+ activation
- Hyperpolarization

1.1.2. Cell model

Cell models are used to obtain insights into the ionic mechanism involved in excitation and inhibition in cell membranes. One of the simplest ways to display a cell as an equivalent electrical circuit diagram is a RC circuit, like shown in fig. 1.3 with its specific conductance values.
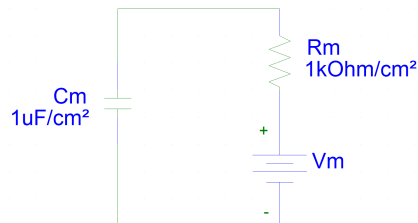
Figure 1.3.: Equivalent electrical Cell model

A value of $1\,\mu\mathrm{Fcm}^{-2}$ is usually used for the specific capacity of a cell membrane. The surface of a cell can then be determined on the basis of the electrically measured capacitance of the entire cell membrane. In practice, the capacitance can be derived from the transient signal generated when charging or discharging the membrane capacitance. Means, the larger the area, the larger the capacitance. The actual capacitance is then (where A is the area of a membrane patch):

$$C_m = C_M \cdot A \tag{1.5}$$

The specific patch resistance of a membrane is $R_M = 1000\,\Omega\text{cm}^{-2}$. The actual resistance is then (where A is the area of a membrane patch):

$$R_m = \frac{R_M}{A} \tag{1.6}$$

With the help of these formulas it is easy to calculate cell capacitances and resistances for various surfaces.

An example of how to calculate the actual cell capacitance and cell resistance of a spherical cell surface

$$C_m = C_M \cdot 4 \cdot \pi \cdot r^2 \tag{1.7}$$

$$R_m = \frac{R_M}{4 \cdot \pi \cdot r^2} \tag{1.8}$$

...where r corresponds to the cell radius. The membrane time constant looks like:

$$\tau_m = R_m \cdot C_m \tag{1.9}$$

There are various mathematical models which deal with the simulation of excitable cells. Below only those models relevant for this work with their corresponding gating variables are presented briefly. **Gating variables** are used to describe ionic membrane currents and cardiac electrophysiology. The dynamics of gating variables are described by the difference between opening and closing rates.

Models of excitable cells

Hodgkin Huxley model (HH model) One of the first models is the so-called Hodgkin-Huxley model. This model is a dynamical model of excitable membranes of unmylenated nerve cells. The model was developed in 1952 by Hodgkin and Huxley [22]. The equivalent circuit of the Hodgkin-Huxley model can be seen in fig.1.4 below.
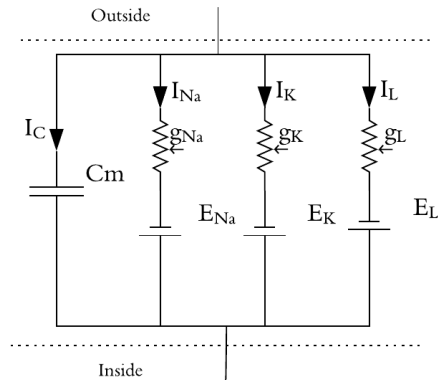
Figure 1.4.: The Hodgkin-Huxley membrane model

The course of an action potential in the Hodgkin-Huxley model can be described by using four different equations. The one calculating the total current shown in eq. 1.10. The three equations left - $\frac{dn}{dt}$, $\frac{dm}{dt}$, $\frac{dh}{dt}$ - describe the gating variables.

$$I = C_m \frac{dV_m}{dt} + I_{Na} + I_K + I_L \tag{1.10}$$

$$I_{Na} = \bar{g_{Na}} m^3 h (V_m - E_{Na}) \tag{1.11}$$

$$I_K = \bar{g_K} n^4 (V_m - E_K) \tag{1.12}$$

$$I_L = \bar{g_l} (V_m - E_i) \tag{1.13}$$

Where $\bar{g_x}$ used in the equation above describe the maximum conductance value of the x_{th} ion channel. All channels are voltage and time dependent, except from the leak channel $\bar{g_l}$. E_K, E_{Na} and E_i are reversal potentials.

The HH action potential course and the corresponding gating variables can be seen in fig. 1.5 and fig. 1.6.
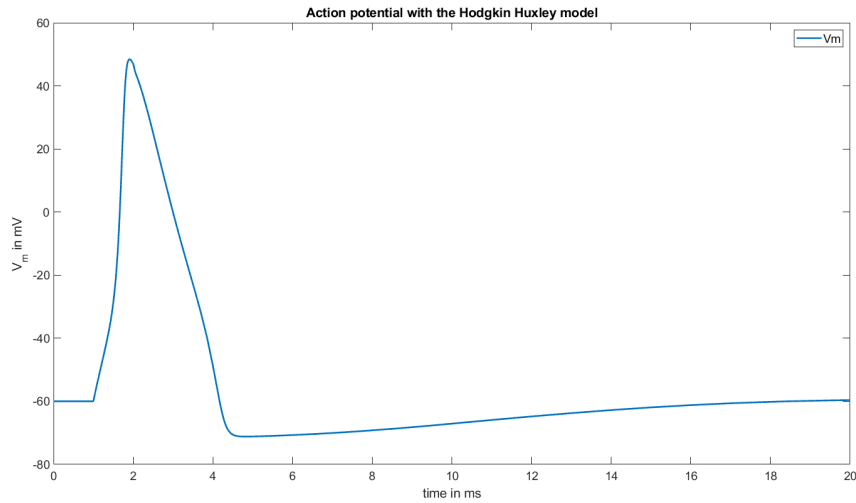
Figure 1.5.: Action potential of a nerve cell with the HH model
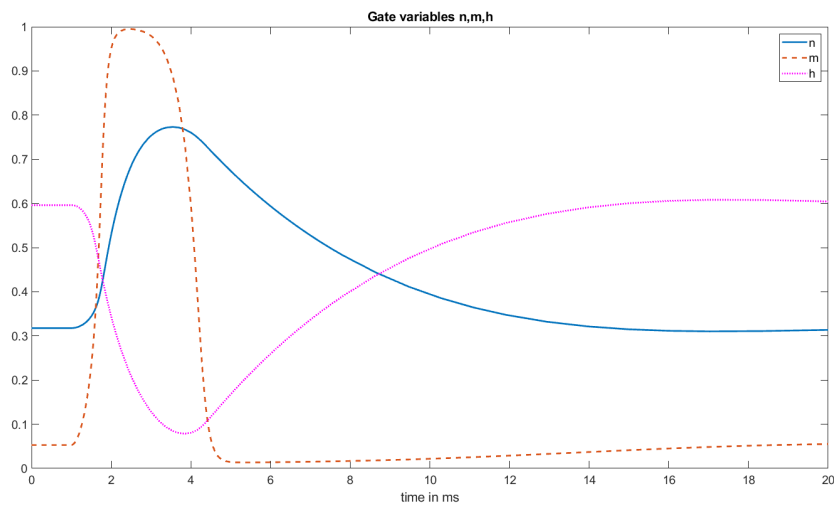
Figure 1.6.: Hodgkin Huxley gate variables

Beeler Reuter model (BR model) Another important model is the Beeler and Reuter Model (1977)[2]. This is an extended HH model developed to describe the electrical activity of the mammalian ventricular myocyte. In this extended model the total current, shown in eq. 1.14, includes four components of ionic currents. The model includes another three voltage-dependent activation variables, three inactivation variables (m, h, j, x1, f and j) and the intracellular calcium concentration ([Ca]).

$$\frac{dV_m}{dt} = -\frac{1}{C_m}(I_{KI} + I_{X1} + I_{Na} + I_{Ca} - I_{ext})\tag{1.14}$$

where

$$I_{ion} = f(V_m, [Ca_i]_i, m, h, j, x1, f, j)\tag{1.15}$$

A schematic representation of a cell membrane with the crossing ion currents crossing are shown in fig. 1.7.
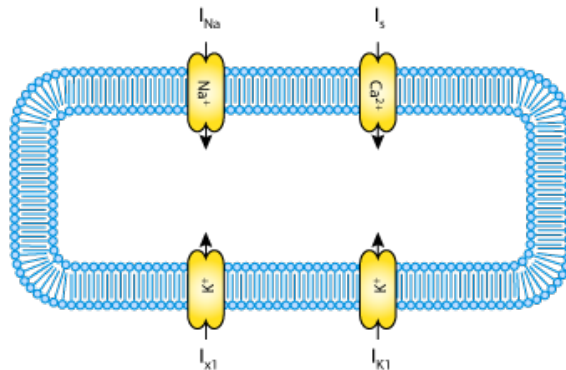
Figure 1.7.: Current flows across the cell membrane in a schematic membrane diagram in the BR model[3]

Luo-Rudy model The Luo-Rudy model (1991) focuses on the interaction between depolarization and repolarization phases of the action potential of mammalian ventricular cells [13]. This model is a more detailed description based on the two already mentioned models. In the BR model there are fixed extracellular ion concentrations, while in the LR model the dependencies of potassium currents on

potassium concentrations are treated. These dependencies have a strong influence on the temporal course of repolarization. A schematic representation of a cell membrane with the crossing ion currents crossing are shown in fig. 1.8.
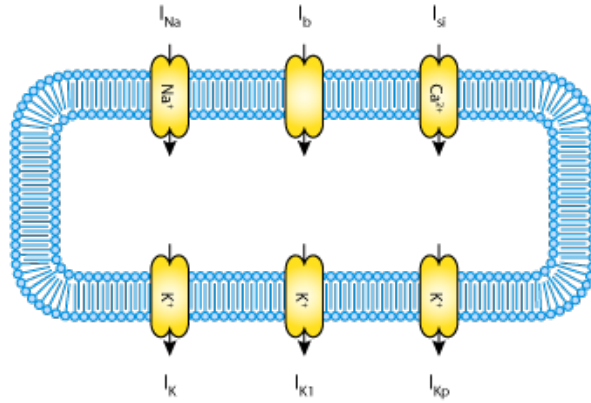
Figure 1.8.: Current flows across the cell membrane in a schematic membrane diagram in the LR model[14]

Ion currents The ion currents important for this model are listed in the equations below, where g_x are the maximum conductances and E_x are the reversal potential of the x_{th} ion channel.

$$\frac{dV_m}{dt} = -\frac{1}{C_m} \cdot (I_{Na} + I_{Si} + I_K + I_{KI} + I_b + I_{stim}) \tag{1.16}$$

Where I_{stim} is the stimulation current used and the single ion channel currents then look like as follows.

$$I_{Na} = (\bar{g_{Na}} \cdot m^3 \cdot j \cdot h) \cdot (V_m - E_{Na}) \tag{1.17}$$

$$I_{Si} = (\bar{g_{Si}} \cdot d \cdot f) \cdot (V_m - E_{Si}) \tag{1.18}$$

$$I_K = (\bar{g_K} \cdot X \cdot X_i) \cdot (V_m - E_K) \tag{1.19}$$

$$I_{KI} = (\bar{g_{KI}} \cdot KI_{inf}) \cdot (V_m - E_{KI}) \tag{1.20}$$

$$I_{Kp} = (\bar{g}_{Kp} \cdot K_p) \cdot (V_m - E_{KI}) \tag{1.21}$$

$$I_b = \bar{g}_b \cdot (V_m - E_b) \tag{1.22}$$

And the gating variables are shown in the following equations:

$$\frac{dm}{dt} = \alpha_m(1 - m) - \beta_m m \tag{1.23}$$

$$\frac{dj}{dt} = \alpha_j(1 - j) - \beta_j j \tag{1.24}$$

$$\frac{dh}{dt} = \alpha_h(1 - h) - \beta_h h \tag{1.25}$$

$$\frac{dd}{dt} = \alpha_d(1 - d) - \beta_d d \tag{1.26}$$

$$\frac{df}{dt} = \alpha_f(1 - f) - \beta_f f \tag{1.27}$$

$$\frac{dX}{dt} = \alpha_X(1 - X) - \beta_X X \tag{1.28}$$

Where α_x and β_x are the opening and closing rates of the x_{th} ion channel. Special voltage dependent conditions for X_i, K_p and KI_{inf} can be found in [13]. The characteristic action potential curve for ventricular cells shown in fig. 1.9 and the corresponding gating variables shown in fig. 1.10, fig. 1.11 and fig. 1.12.
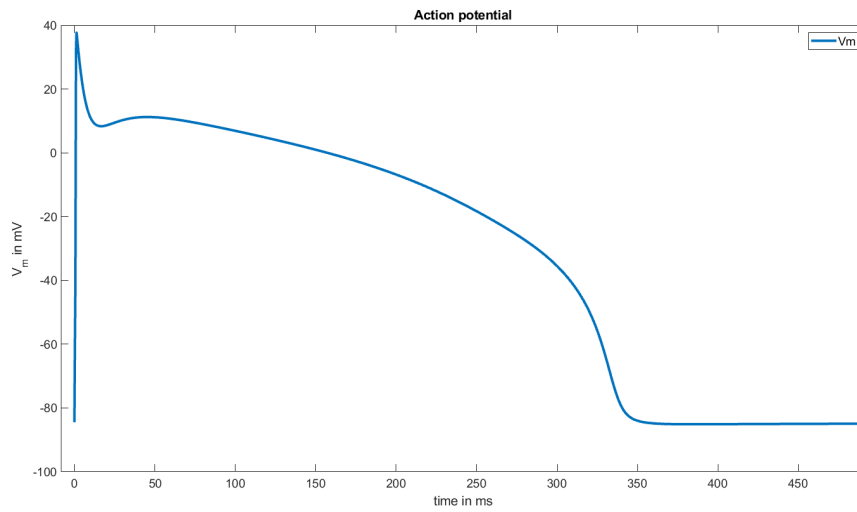
Figure 1.9.: Action potential of a ventricular cell with the LR model
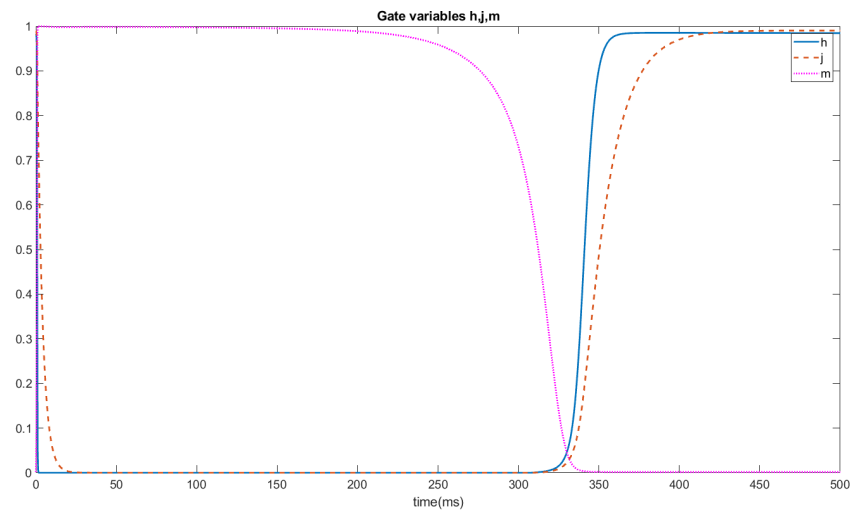
Figure 1.10.: Luo-Rudy gate variables h,j and m

1. Introduction
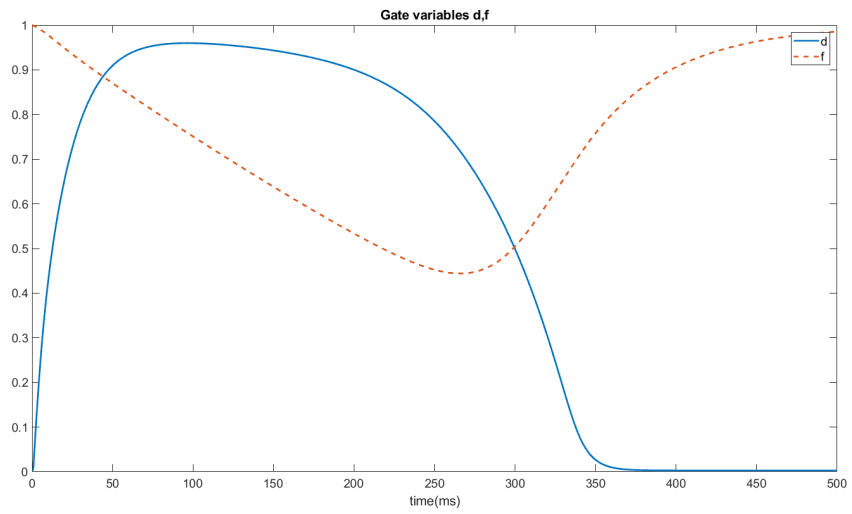
Figure 1.11.: Luo-Rudy gate variables d and f
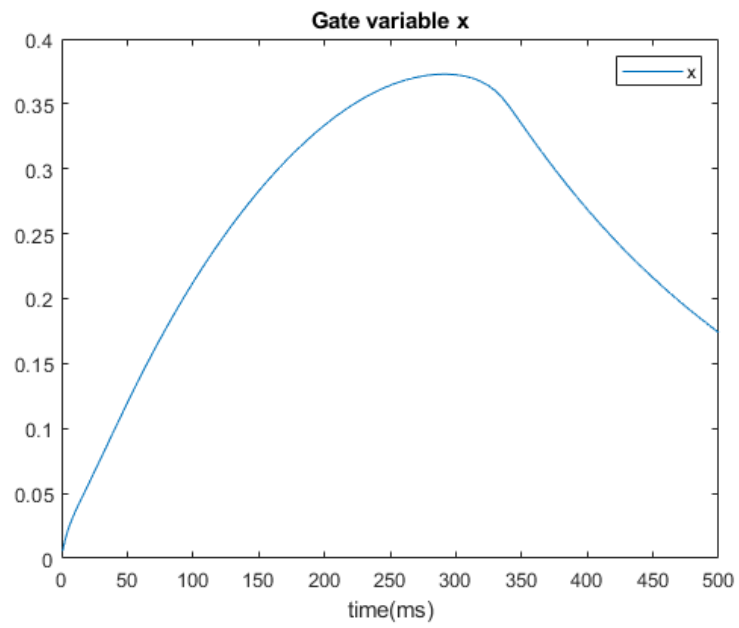
Figure 1.12.: Luo-Rudy gate variable X

1.2. External Stimulation

There are mainly two ways how cells can be stimulated. One possibility would be current injection and the other one would be via external field stimulation. External stimulation has the great advantage that it is a less invasive method. It also eliminates the need for wiring. Actually, the activation by an electric field differs in many ways from the activation by intracellular injection of stimulation current, shown in table 1.1.

Table 1.1.: Stimulation of cardiac cells at normal resting potential by extracellular electric fields, compared with stimulation by intracellular current injection; modified from [29]

	Extracellular field	Intracellular current
Transmembrane potential	Nonuniform	Uniform
Stimulus polarity	Independent *)	Dependent
Source of depolarizing	Ionic currents	Stimulating cathode and ionic currents
I_{Na} **during pulse**	Large amplitude	Small amplitude
I_{K1} **during pulse**	Can be inward	Outward only
Phases of symmetrical biphasic pulse	Synergistic	Antagonistic
Symmetrical biphasic vs. monophasic pulses *2)	Similar	Less effective

*) (for uniform field and cells symmetrical about the equator) *2) having same total duration

The aim is, when an excitable cell is placed in an electric field, to create an electromagnetic coupling between the cell and the field. This should then trigger an action potential. Means the cell activation should be caused by the external field stimulation.

1.2.1. Types of external field stimulation

Essentially, electric fields can be described as **homogeneous** and **non-homogeneous** fields. A homogeneous field would be optimal, since this shows an optimized behavior by in parallel oriented field lines which are equally distributed, shown in fig. 1.13. In an in-homogeneous electric field, shown in fig. 1.14, field lines are prone for a curved line-shape and are concentrated near edges and next to charges. In this work, an external stimulation with a non-uniform electric field is used.

Figure 1.14.: Non-uniform electric field [20]

Figure 1.13.: Uniform electric field

1.2.2. Stimulation modes

This short chapter compares different types of stimulation:

- Monophasic vs biphasic stimulation mode, and
- Rectangular vs ramp stimulation

In this work, a biphasic stimulation current is used, starting from a light controller triggered by a rectangular pulse. Reasons for doing it in this way are stated in the following sections.

Monophasic vs biphasic stimulation

Monophasic stimulations require a particular amount of charge to be applied over a certain timeframe in order to stimulate a cell. In case of monophasic stimulation, it is also referred to as a linear phase, whereas in the case of biphasic stimulation non-linearities play a major role. Biphasic stimulation begins with the so-called stimulation phase. That phase is responsible for triggering an action potential in excitable cells. The second phase of a biphasic pulse is known as the reverse phase. During the stimulation phase, it is responsible for the inversion of electrochemical processes. In biphasic stimulation it is typical that the stimulation pulse is a so-called cathodic pulse (the working electrode is operated negatively), while the reverse phase corresponds to an anodic phase (working electrode is operated positively)[27], [18], [24].

The research referenced to [31] shows that biphasic stimulation may be more suitable for defibrillating cells than monophasic pulses. They damage cells less during a shock, but are often less able to stimulate a cell than a monophasic pulse. In this research a 10-ms monophasic stimulation pulse was compared with a 5/5-ms biphasic stimulation pulse. The experiment shows that the biphasic wave pulse causes less conduction blocking than a monophasic wave pulse would.

Rectangle vs ramp stimulation

In the latest publication on Photocaps, the difference in light control between square-wave pulses and ramp pulses was compared[8]. While a ramp pulse resulted in a longer transient voltage, the Photocap could not reach the same maximum photovoltage when excited by a ramp pulse as it would with a square wave pulse, shown fig. 1.15. Light intensity ramps can be used to obtain a longer lasting voltage transition. The ramp shape of the light intensity leads to a nonzero derivation of the charge current dI/dt therefore the transient voltage in electrolyte persists. Although the rest of the curve shown in 1.15 was larger at the end of the light pulse when using a light ramp shape, nevertheless the capacity of a Photocap could be increased in better way when using PEDOT:PSS.
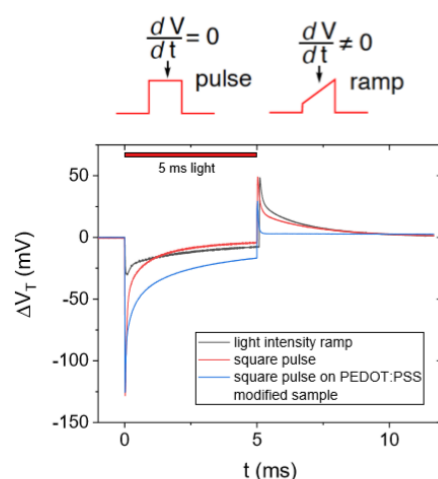
Fig. S6. Comparison of voltage transients in the case of light intensity ramps with a

Figure 1.15.: Comparison of voltage transients in case of light intensity ramps with a standard light pulse [8]

1.2.3. Charge transfer: faradayic and non-faradayic currents

If a voltage is applied between two electrodes, a current flows. There are two reasons that may be responsible for this procedure. On the one hand there can be the exchange of electrons between the electrode and substances in the solution, i.e. there is a charge transition between the electrode and the solution (Faraday current). The other case is caused by charging the electrolytic double layer (capacitive current). An electrolytic double layer is formed at the electrode/solution boundary. If the electrode is negatively charged (cathode), the positively charged cations accumulate predominantly in the solution in front of the electrode. The electrolytic double layer (negatively charged electrode/positively charged boundary layer of the solution) is comparable to a capacitor[18].

Neglect of the faraday current
Since the idea of this project is based on the first two publications about Photo-caps[9][8], the faraday current can also be neglected in this project, refering to following quote: "ITO was favorable as it has a high overpotential for undesired faradaic processes (35), unlike gold, which can more easily catalyze various redox reactions" [9].

1.2.4. Cells in non-homogenous fields

When a cell is placed in an electric field, it becomes polarized: depolarized/positive at the end of the cell facing the cathode to hyperpolarized/negative at the other end facing the anode. The cell excitation depends on the orientation of the cell in the electric field[29],[11].

One of the main advantages of extracellular field potential stimulation is that this method allows non-invasive electrical investigations since no intracellular electrodes are used and thus the intracellular environment of the cells remains unaffected. The suitability of different stimulation mechanisms varies according to the desired application. The approach is that for effective extracellular stimulation a certain charge threshold has to be delivered to the cell.

Calculation of the electric field distribution in non-homogeneous electric fields

The spatial and temporal distribution of the membrane voltage generated by an external electric field is determined by the shape of the cell, its membrane and cell properties and the orientation of the cell in the extracellular electric field. The distribution of field potentials in extracellular space is influenced by the presence of cells, especially if they have a larger volume. This violates the assumptions of classical cable theory, which tries to describe electrical currents and potential differences along passive nerve fibers using mathematical models. Another important factor in the calculation of the non-homogeneous field is the electrode-cell spacing. Intra- and extracellular potentials are assumed to be purely resistive, with corresponding conductivities. It follows that the intra- and extracellular potentials fulfill the equations of Laplace.

On the other side, the membrane tension generated by a **uniform electric field** can be dissolved by Swan. Here the voltage follows a cosine function along the cell membrane, shown in eq. 1.29. In addition, it is proportional to cell size and field strength[12]. The maximum transmembrane potential is:

$$\Delta\psi_{\text{membrane}} = 1.5aE_{\text{appl}}\cos\Phi / [1 + (\omega\tau)^2]^{1/2} \tag{1.29}$$

where a is the radius, E_{appl} is the oscillating field and Φ is according to following quote: "...Φ is the angle between the field line and a normal from the center of the sphere to a point of interest on the cell membrane."cited from [16]. τ is according to following equation:

$$\tau = aC_{\text{membrane}}(\rho_{\text{int}} + \frac{\rho_{\text{ext}}}{2}) \tag{1.30}$$

where ρ_{int} and ρ_{ext} are the resistivities of the internal and external fluid.

1.3. Photocaps

The Photocap, shown in 1.16, is a novel technology for neuronal stimulation. It has the ability to convert a light pulse into a capacitive current.

Figure 1.16.: Picture of a Photocap

The device has a diameter of about 30 mm and consists of different layers with different properties, which fullfill different tasks. A schematic representation which shows the structure of the Photocap can be seen in fig. 1.17.
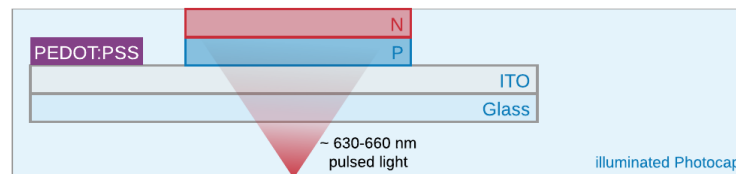
Figure 1.17.: Schematic layer structure of a Photocap

The layers are described from the bottom layer to the top layer.

- **Light Source:** located underneath the Photocap, in the wavelength range of 630 nm to 660 nm.
- **Glass:** 1.1 mm thick borosilicate glass[8]

- **Indium tin oxide (ITO):** Semiconductor with a thickness of about 100 nm, typically a resistance of about 15 Ω. An ITO coated float glass with 100 nm has a transmission of approx. 84...89% in the visible wavelength range (400 nm to 700 nm) [6], [7].
- **PEDOT:PSS**: PEDOT:PSS increases the charge density of the Photocap, PEDOT:PSS is used as an electrochromical material, which means that molecules and crystals can change their optical properties by an external electric field or current flow. The absorption is increased between 550 nm and 650 nm in the reduced state, where PEDOT then becomes dark blue[25].
- **PN layer:** Organic photoconductor nanocrystalline, consisting of organic materials, shown in 1.18. The **PN layer is the core of a Photocap** and is responsible for the transformation of a light pulse into a capacitive current. One of the reasons for this high-performance electricity is that the organic molecules used are very efficient absorbers. PTCDI forms the N layer and is an organic molecule used in the research and development of organic semiconductor devices and commercially manufactured by the pigment industry [17]. While H2Pc forms the P layer and is characterized by high chemical and thermal stability and resemble to related classes of organic dyes.
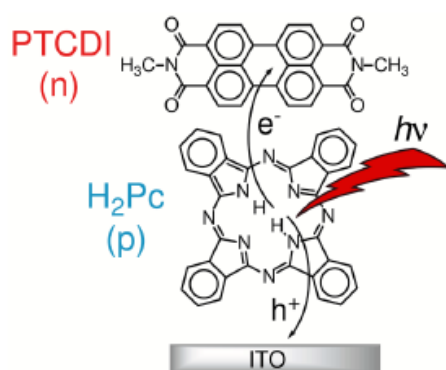
Figure 1.18.: Schematic structure of a PN layer

1.3.1. External stimulation induced by a Photocap

A Photocap is the source that generates a non-homogeneous electric field from which cell stimulation is initiated. The functionality of a Photocap is like described in "non uniform fields" in Section 1.2.1. The external stimulation set-up involving the Photocap behaves like a 3-electrode measuring system, which generates a non-homogeneous electric field originating from the Photocap. The Photocap works in this measuring setup as so-called working electrode and the measuring pipette as counter electrode. A third electrode is used as a reference electrode, which, as the name suggests, serves as a reference in measurements[18].

2. Tasks

The idea for this project comes from a project called "LOGOS-TBI", which means: **L**ight-controlled **O**r**G**anic semic**O**nductor implant**S** for improved regeneration after Traumatic Brain Injury. This is a cooperation project between the Medical University of Graz and Graz University of Technology. TBI may destroy the functions of the brain, either temporarily or permanently. All levels of TBI involve the risk of significant long-term disability. Apart from physiotherapy, there are still no long-lasting therapeutic possibilities to restore the regeneration of such functional deficits. The idea of the LOGOS-TBI project is to explore an alternative therapy for the regeneration of such functional deficits. So-called light-activated Photocaps provide neuronal cell stimulation and should eventually lead to neuronal cell regeneration and TBI protection.

The task of this master thesis is to generate a simulation model for excitable neuronal and cardiac cells. The stimulation of these excitable cells should be generated with the abovementioned novel technology, the Photocap. In order to later obtain the parameterization for the model, a characterization of the Photocap is necessary. This has to be guaranteed by so-called eletrical photoresponse measurements (EPR Measurements; known from [8]) as well as electrical field potential measurements. The entire measurement setup, from stimulation via a light source, the light excited Photocap, the excitable cells, right up to the measurement of the membrane voltage via the Patch Clamp system, should then be represented in an equivalent circuit diagram. Furthermore, a simulation of action potentials of the cells should be performed in Matlab.

The Photocap experiments with living cells will be carried out with chicken cardiomyocytes by the staff of the Medical University. Chicken cardiomyocytes have some advantages, e.g. a longer action potential duration and a spherical cell shape, which is especially easier for first modelling attempts than working with unshaped neurons.

2.1. Characterization of the Photocap

Electrical **P**hoto**R**esponsone and electrical field potential measurements should be carried out to characterize the photocharging dynamics of such a device[8]. Parameters like the stimulation voltage, the resulting stimulation current, the droplet size and many other important characteristics will be incorporated in the developed cell model for optimisation. Only by measuring the practical behavior of the Photocap reasonably realistic values can be obtained in a model.

2.2. Model for excitable cells

In addition to a clear equivalent circuit diagram of the cell structure during stimulation, a detailed action potential cell model for chicken cardiomyocytes, should be developed. The stimulation of these cells takes place in an electric field. Using this cell model, meaningful statements on strength duration values, threshold voltages and other similar parameters will be derived. The theoretical values should in the end be compared with practical values.

2.2.1. Equivalent circuit model

The equivalent circuit diagram should cover the entire measurement setup as well as following parts: Electric photoresponse measurement, electric field potential measurement and cell measurements with patch clamp. Splitting into several circuit diagrams should help to have a better understanding of the entire measurement setup and the working principle of a Photocap.

2.2.2. Action potential simulation of excitable cells

A mathematical cell model should be developed to find out whether it is theoretically possible to stimulate cells growing on a Photocap. The most suitable model for the specific cell type should be chosen. Information about the action potential progression, gating mechanisms and ion currents should be provided. Parameters from the previously created equivalent circuit should be included in the implementation in order to obtain even more realistic values.

3. Methods

In this thesis, the model of excitable cells stimulated by a Photocap is divided into two essential parts: The first part is an equivalent circuit implemented in PSpice which represents the measuring with a Photocap. The simulation in PSpice is split into separate sub-simulations. Some of those sub-simulations are in the end combined to one whole model. The second part is the implementation of a theoretical cell model in Matlab.

In fig. 3.1 a schematic representation of the entire measurement setup is shown. Sub-measurements and simulations can always be derived from this representation in a simplified form.
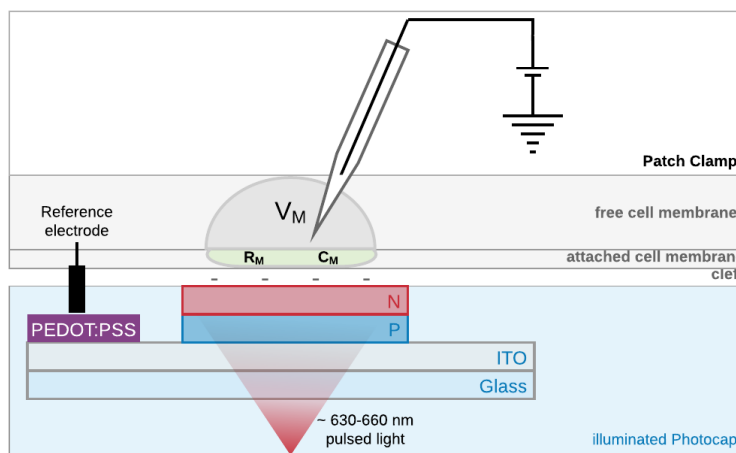
Figure 3.1.: Schematic representation of the entire measurement setup

The origin of the idea for the technical structure of this schematic representation is explained in the following subsections.

3.1. Characterization of the Photocap

This chapter describes the methodology required to characterize the behavior of a Photocap, via

- **E**lectrical **P**hoto**R**esponse measurement (EPR) and
- Field potential measurement (FP)

The following specifications apply to both measurement methods listed above:

Distance In all the measurements used to characterize the Photocap, it applies, that the closer the measuring pipette is located to the Photocap, the better the measuring resolution[8].

LED An LED is operated in the wavelength range between 630 nm and 660 nm. The distance between LED and Photocap should be kept as small as possible.

Electrolyte solution A highly concentrated 3 M KCl solution is often used as an electrolyte solution. This kind of solution is used for an EPR measurement as well as for the field potential measurement. In the latter measurement a 3 M KCL solution is used in the measuring pipette as well as in the electrolyte bath, since it has a good conductivity and therefore a lower resistance than measuring with different solutions, e.g. in- and external cell solutions.

3.1.1. EPR measurement

In an electrical photoresponse measurement the Photocap is illuminated and excited from below. In this measurement, the maximum voltage that can be generated by a Photocap is measured between the measuring electrode (located in the 3 M KCL filled glass pipette) and a reference electrode (connected with the PEDOT:PSS). An electrical connection is established via an electrolytically conductive drop between the pipette tip and the PN layer of the Photocap. While fig. 3.2 shows the schematic construction, fig. 3.3 shows a picture of the measurement setup found in practice.
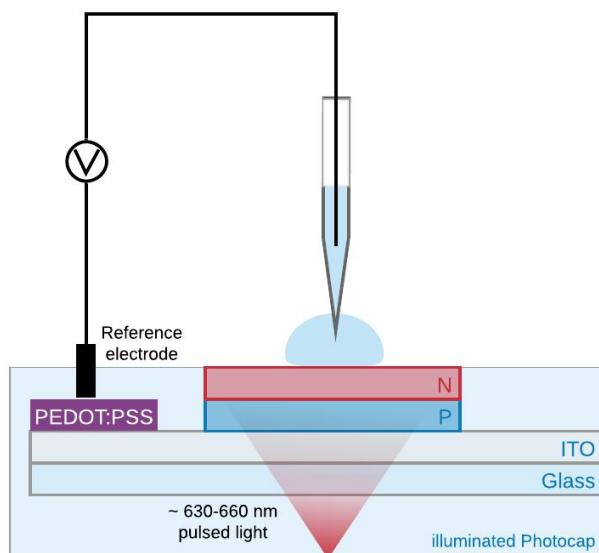
Figure 3.2.: EPR measurement setup
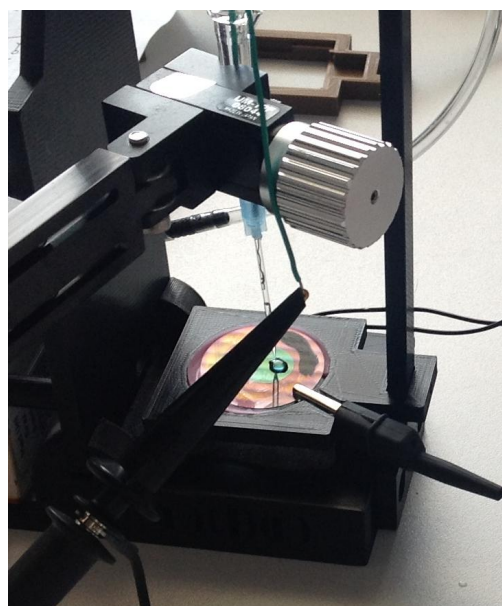
Figure 3.3.: Picture of the EPR measurement setup

So-called micro electrodes are required for the EPR measurement. Glass capillaries are therefore pulled out to fine pipettes with tip diameters of less than 0.5 µm. These pipettes are used to form drops in the µm range as electrical contact between the measuring electrode and the Photocap. The electrical contact is also established via an electrolyte solution in the pipette and an AgCl compound. An AgCl-coated bath electrode serves as a reference.

Drop The electrolyte drop can either be pipetted or squeezed out of the measuring pipette via a syringe by adding pressure. Droplets in this measurement setup usually have a standard droplet size. A standard droplet has a length of about 2.5 mm and 50 µl (=0.05 ml).

3.1.2. Field potential measurement

The following pictures show on the left side (fig. 3.4) a schematic representation of a measurement setup for quantifying the field potential, while on the right hand side a picture of the measurement setup with a Photocap floated in a 3 M KCL solution can be seen (fig. 3.5). The LED, which excites the Photocap by light pulses, is located below the device. The measurement is carried out using a Patch Clamp system: In voltage clamp mode the pipette offset has to be done at the beginning. Then the voltage is measured in the current clamp mode (with I=0) in the bath via a measurement electrode (which is located inside the pulled glass pipette). The reference electrode is suspended in the bath during the measurement. The electric field potential measuring is then carried out at different positions (of the measuring electrode) in the bath.
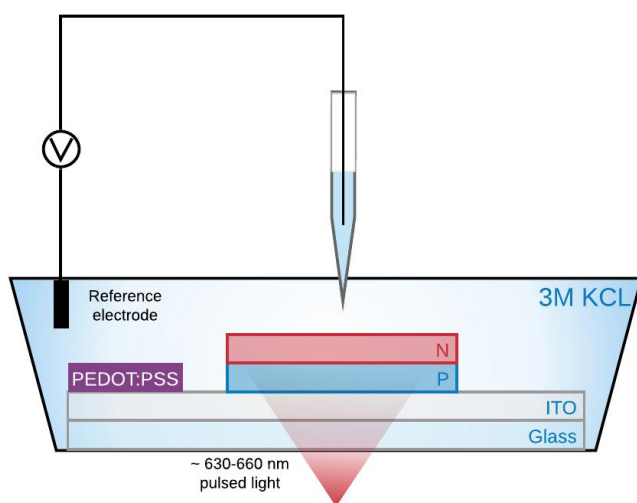
Figure 3.4.: Field potential measurement setup
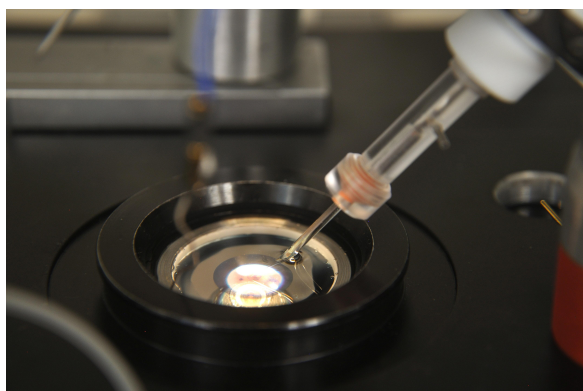
Figure 3.5.: Field potential measurement setup with a Photocap floated in a 3 M KCL electrolyte

3.2. Equivalent circuit diagram

The development of suitable equivalent circuit diagrams is mainly based on two sources, the **Electrical Impedance Spectroscopy** and the **Two-Domain-System**. The idea for the equivalent circuit design of Photocaps comes from the **Electrical Impedance Spectroscopy (EIS)**. Resulting circuits of an EIS are based on so-called "Randles circuits"[19]. The easiest form of a Randles circuit consists of a solution resistance, a double layer capacitance and a charge transfer capacitance, shown in fig. 3.6. The component **Z**, shown in bottom of the figure, stands for the diffusion component which can again be divided into the **Warburg impedance** Z_w (infinite diffusion thickness) and in **T, O and G elements** $Z_{O/T/G}$ (finite diffusion).
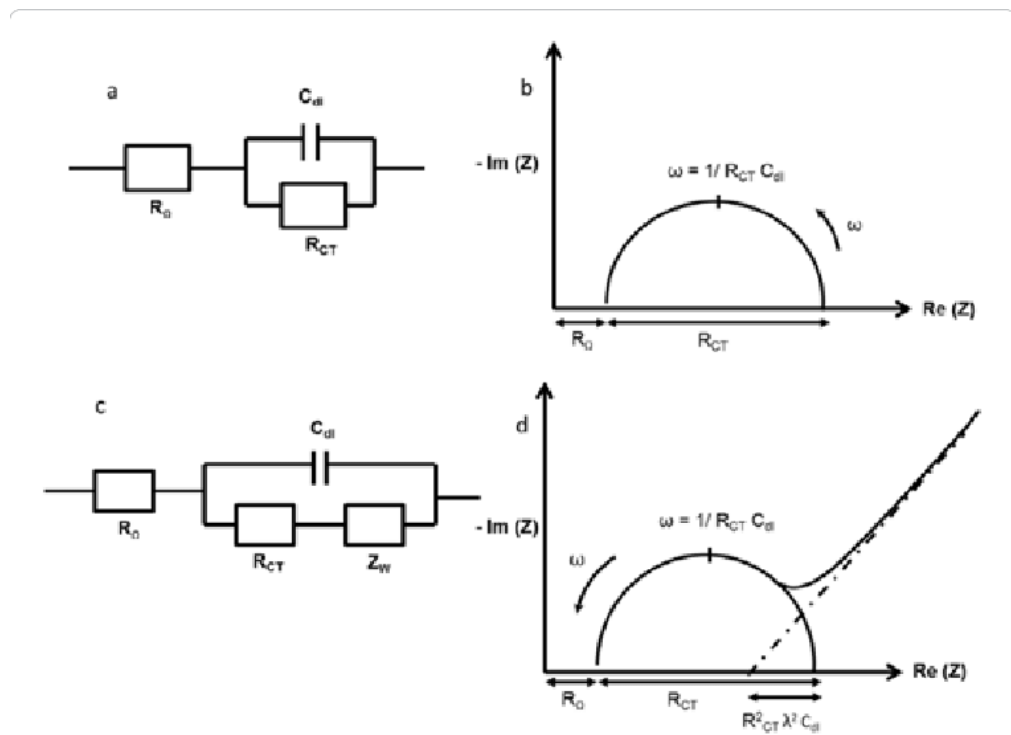
Figure 3.6.: Representation of Randles circuit cited in [19]

The result of an EIS procedure provides information about the behavior of devices in certain frequency ranges. In the first publication about Photocaps[21] an EIS was executed. The idea when implementing an equivalent circuit is to use same

component parts like shown in fig. 3.7 in a very similar arrangement, but different component sizes. The component sizes should be chosen in such a way that the simulation in the end corresponds with the measured values in reality. research team carried out
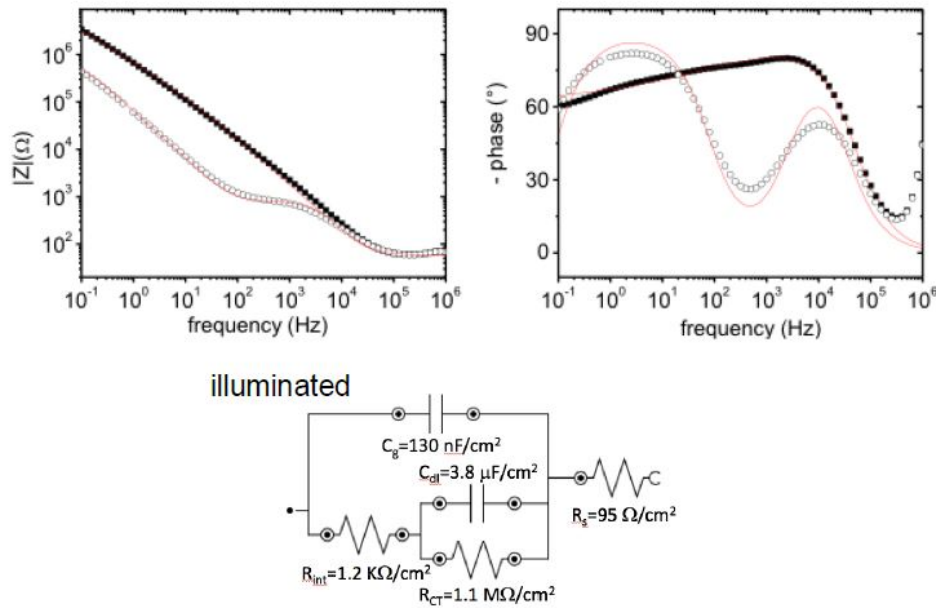
Figure 3.7.: EIS: open circles (illuminated Photocap), black squares (measured in dark) [21]

The second source which led to the idea for implementing an equivalent cell circuit with a so-called **Two Domain System (TDS)** is provided by Ingmar Schoen and Peter Fromherz, with reference to [24]. Their idea for a TDS is shown in fig. 3.8 below. Their research was done in a very similar application, namely the stimulation of nerve cells on an electrolyte-oxide-semiconductor capacitor. As already described in Chapter 1.2.4, a different polarization occurs within a cell at opposite cell ends when a cell is positioned in a non-homogeneous electric field. Schoen and Fromherz therefore had the idea to divide an excitable cell in the model into two parts, specifically the part that is directly excited (the attached cell part) and the cell part that is not directly affected by the stimulation (the so-called free membrane).

3. Methods
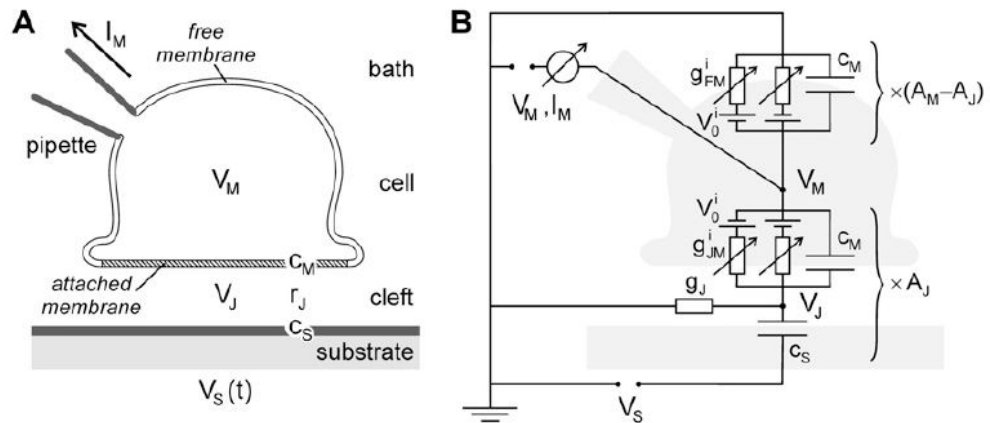
Figure 3.8.: TDS Model [24]

Following table describes the single elements used in the figure above, which show a nerve cell on a capacitor where a TDS model is used. The cleft has a height of about 20nm.

Table 3.1.: Description of elements shown in 3.8

I_M	Membrane current (measured or controlled)
V_M	Membrane potential
C_M	Area-specific capacitance
V_J	Extracellular voltage
r_J	Sheet resistance
c_S	Substrate capacitance
$V_s(t)$	Applied voltage ramp
g_{FM}^i	Ionic conductances, free membrane
g_{JM}^i	Ionic conductances, junction membrane
V_0^i	Reversal voltages
A_M-A_J	Free membrane area
A_J	Attached membrane area

An overview of an overall schematic representation of an equivalent circuit design can be seen in fig. 3.9. This representation combines the two large individual parts: the illuminated Photocap and the TDS of the cell. A Patch Clamp was also considered in this overview, since the membrane voltage is measured by such a system, which are driven either in Voltage Clamp or Current Clamp mode.
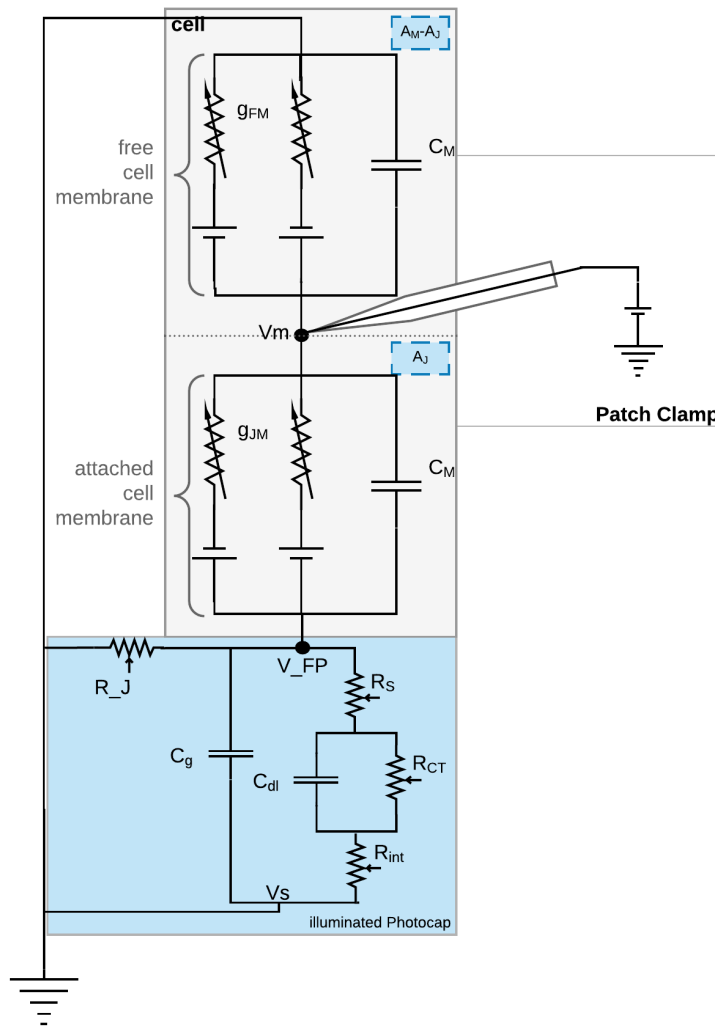
Figure 3.9.: Comprehensive schematic equivalent diagram of the Photocap-cell-measurement setup

Used parameters in the equivalent circuit diagram are described in table3.2 below. The equivalent circuit diagram is a simplified representation. The exact implementation of this circuit is shown and discussed in the Results4 and Discussion5.

Table 3.2.: Parameters used in the equivalent circuit diagram, shown in 3.9

V_s	Applied voltage ramp to the substrate
R_{int}	Internal resistance of the illuminated PN junction
C_{dl}	Capacitance between the PN layer and the electrolyte
$R_{CT} > 1.1\,M\Omega cm^{-2}$	Charge-transfer resistance
R_S	Serial resistance acc. to the electrical resistance of electrode material and electrolyte
R_J	Resistance of the junction width
V_{FP}	Electrical field potential
A_J	Area of the **attached membrane**/ the directly stimulated part of the cell
A_M - A_J	Area of the **free membrane**/ the indirectly stimulated part of the cell
C_M	Membrane capacitance
g_{JM}, g_{FM}	A summed representation of all ion channel conductivities used in the attached cell membrane (suffix JM) and the free cell membrane (suffix FM).
V_m	Membrane voltage

Patch Clamp
Patch clamping is used for cell measurements, either in Voltage or Current Clamp mode. In addition, the Patch Clamp system is used as an alternative measurement method to measure the electric field potential, as described in 3.1.2.

3.3. Action potential simulation of excitable cells

To simulate excitable cells using a stimulation current, a model according to Luo Rudy and Ebihara Johnson is implemented. In an earlier research of finding the activation thresholds for chick heart cells, different combinations of models were tested[26]. The aim of this research was to find the model combination that predicted the most realistic threshold voltage (closest to the experimentally measured threshold voltage). In summary, the combinations of the Luo Rudy and Ebihara Johnson models were able to achieve the best simulation results. In addition to physiological parameters that apply to chicken cardiac cells, parameters such as the fast sodium channel are also adapted in the model[4].

> Adjusted parameters when using chicken cardiac cells
>
> - **Resting membrane potential:** $V = -70\,\mathrm{mV}$
> - **Activation threshold:** $K_e = 5.55\,\mathrm{mM}$ instead of $6.5\,\mathrm{mM}$ (LR model)
> - **Internal sodium concentration:** $Na_i = 40\,\mathrm{mM}$
> - **External sodium concentration:** $Na_e = 140\,\mathrm{mM}$
> - **Specific cell capacitance:** $1\,\mathrm{\mu Fcm^{-2}}$

Comparison of predicted threshold voltages (mixed models) and the experimental measured threshold voltage, shown in fig. 3.10.

Figure 5. *Activation thresholds measured experimentally (———) and predicted by the cell models with Ebihara-Johnson/Lou-Rudy (— —), Ebihara-Johnson/Shrier-Clay (− − −), and enhanced Ebihara-Johnson (- - - -) membrane dynamics.*
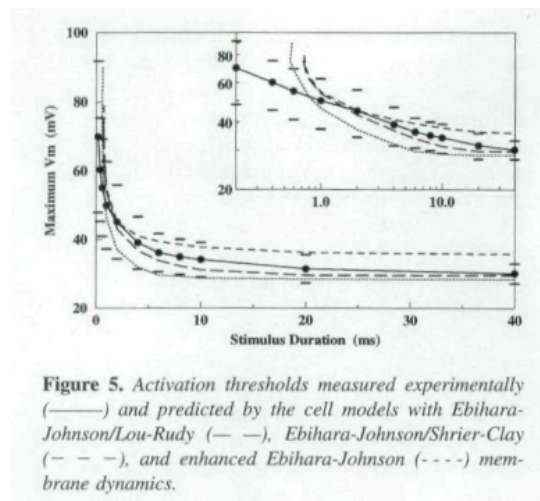
Figure 3.10.: Threshold measured compared to predicted models[26]

3.3.1. Luo Rudy Ebihara Johnson model parameters

While the fast sodium current from the Ebihara Johnson model is used (without the j gate), shown in eq. 3.1, the other currents are used according to the Luo Rudy model, like shown in 1.1.2. Table 3.3 lists the parameters to be considered for this model.

$$I_{Na} = (\bar{g_{Na}} \cdot m^3 \cdot h) \cdot (V_m - E_{Na}) \tag{3.1}$$

Furthermore, for the implementation of this mixed model it should be noted that in the paper which served as a basis for this thesis, a homogeneous electric field was used, while in this thesis a non-homogeneous electric field and biphasic impulses are used.

Table 3.3.: Luo-Rudy Ebihara Johnson parameters for the chicken cardiomyocyte model [13] [5]

$I_{Na}[\mu A/cm^2]$	Fast sodium current
$I_{Si}[\mu A/cm^2]$	Slow inward current (same as in BR-model)
$I_K[\mu A/cm^2]$	Time-dependent potassium current
$I_{KI}[\mu A/cm^2]$	Time-independent potassium current
$I_{Kp}[\mu A/cm^2]$	Plateau potassium current
$I_b[\mu A/cm^2]$	Background leakage current
$V_m[mV]$	Membrane potential
$E_i[mV]$	Reversal potential of ion i
m	activation gate of I_{Na}
h	Fast inactivation gate of I_{Na}
d	Activation gate of I_{Si}
f	Inactivation gate of I_{Si}
x	Activation gate of I_K
X_i	Inactivation gate of I_K
K_I	Inactivation gate of I_{KI}
α, β	Opening and closing rate constants of gate i
τ_i	Time constant of gate i

3.3.2. Strength-duration curve

The Strength-duration curve indicates the time or current required to trigger an AP. The stimulation curve (time over current/voltage) is the threshold curve for rectangular stimulus pulses, which has a hyperbolic character. A characterization for the mixed model of Luo Rudy and Ebihara Johnson is carried out.

A typical representation of a strength duration curve is shown in fig. 3.11.
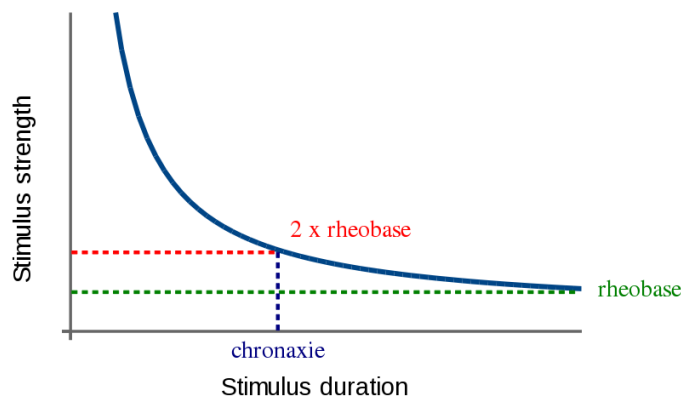
Figure 3.11.: Strength duration curve with marked rheobase and chronaxy with reference to [1]

Rheobase: Is the minimal current/voltage at infinite duration which elicits an action potential
Chronaxy: Threshold pulse duration at 2x rheobase

3.3.3. Stimulation frequency

While the strength duration curve is used to find out how long and intense a pulse should be that an action potential can be triggered, an optimized **stimulation frequency** should be found in a comprehensive characterization phase. Means the relationship of a perfect pulse-intra-pulse duration should be determined.

4. Results

4.1. Characterization of the Photocap

For the Photocap measurements two different types of measuring systems were used, which can be seen in the pictures 4.1 and 4.2, as well as two different oscilloscopes, the **RS Pro RSDS 1204CFL, 200 MHz** and **DSOS054A High-Definition Oscilloscope: 500 MHz**. In order to be able to carry out experiments at the Graz University of Technology, a separate experimental setup was built for the laboratory at the iHCE. An detailed description can be seen in 4.1.1.

Figure 4.1.: 3D printed measurement assembly

Figure 4.2.: Measurement setup included in a Zeiss microscope at the Medical University of Graz

4. Results

The field potential measurement was done with the help of the Patch Clamp measuring devices

- Axopatch 200B
- Axon Digidata 1550

which were available at the Medical University of Graz..

At the Medical University of Graz were two almost identical workstations which could be used for the Photocap experiments. One was in a Faraday cage, like shown on in fig. 4.2 while the other was not. In the latter setup the LED to be controlled was built into an **Axiovert 10 microscope objective**, while in the other setup the LED was included in a Zeiss microscope objective.

The measuring electrode construction consisted of finely pulled glass pipettes, which were filled with 3M KCL. The electrode itself was located in this filled glass pipette. The raw material were glass tubulars called **30-0068 Glass capillaries GC150TF-7.5**. A readily prepared measuring pipette is shown in fig.4.3.

Figure 4.3.: Fully prepared measurement pipette

This chapter shows the results that led to the characterization of a Photocap. At the beginning an **electrical photoresponse measurement** was performed, which is supposed to deliver the maximum voltage generated by a Photocap. Then the **measurement of the electric field potential** was proceeded to obtain on the one side information about the distribution of the electric field in an electrolytic bath and on the other side to get an idea of the voltage that would approximately reach a cell.

4.1.1. Reproduction of the experimental setup

As described above, a separate experimental setup was made for the iHCE labora-
tory. The LED controller was manufactured in the context of a separate Bachelor
thesis and could be used for the measurement experiments. Since EMC interfernces
and bad influence by ambient light repeatedly occurred during measurements at
the Medical University of Graz, the aim was to build a measurement setup as flexi-
ble as possible for the laboratory at the iHCE. A small and portable setup needed
to be developed that could be set up quickly at any location. Due to the flexible
requirements it was decided to make a 3D print. This chapter briefly describes
the individual components that were produced for this purpose. The 3D printed
construction is shown in fig. 4.4. [15] served as basis for the fundamental structure
of this measurement setup. Holders and other accessories had to be designed
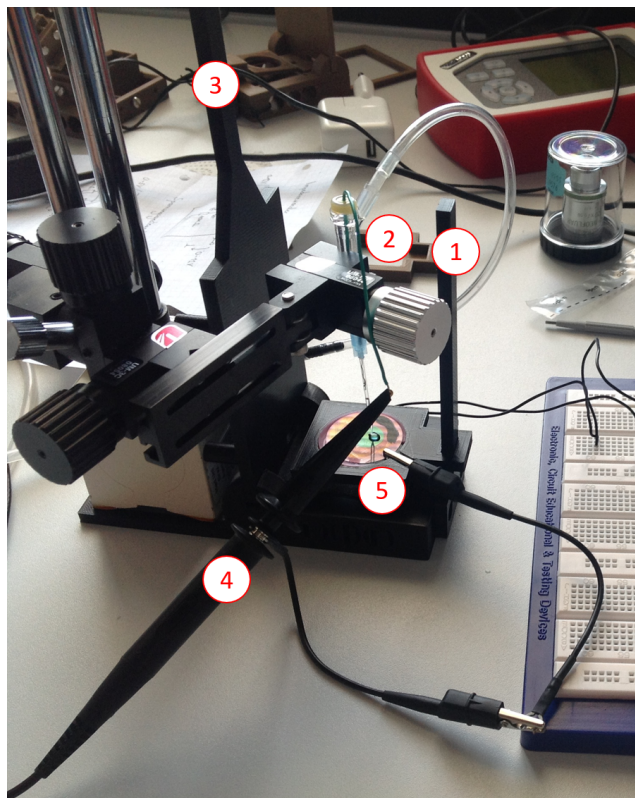according to the requirements.

Figure 4.4.: 3D printed measurement setup

4. Results

In addition to a central opening in which the LED can be placed, the basic framework also contains a rod on which the cup holders (Photocap support) can be positioned at different heights. Marked points in fig. 4.4 are explained below:

- **1...Rod:** Rod for Photocap holders
- **2...Pipette holder:** The pipette holder is a so-called needle-free Y-system that is normally used e.g. for plasma dispensing. The advantage of this system is that it has two airtight supply points. One supply (at the top) is sealed airtight by a membrane. The AgCl coated measuring electrode was inserted through this membrane and finally positioned in the glass pipette. The signal can now easily be picked up at this measuring electrode during the measurement. The glass pipette is an independent measuring accessory that has to be attached prior to the measurement. New glass pipettes are used for each measurement series, because these are filled with highly concentrated electrolyte, which crystallizes very quickly and clog the fine pulled pipettes. This means that these pipettes are unsuitable for repeated use. The glass pipette is therefore an independent part of this measuring construction and can be easily removed and attached. The other supply is located laterally and is connected to an air-filled syringe via a piece of tube. Thus, the electrolyte liquid level in the filled glass pipette can easily be regulated by this external pressure control. This means that droplets can generated by this external pressure control system as well as reduced in size (by pushing or pulling on the syringe).
- **3...Additional rod:** An additional holding rod which could be used to mount a camera or similar from above.
- **4...Oscilloscope probe:** The probe can easily be connected to the measuring cable that is led out of the pipette.
- **5...Photocap holder:** Different Photocap holders, according to different measurement types (EPR, FP), were constructed. The Photocap holder for EPR measurements is shown in 4.5. The holder for field potential measurements is shown in fig. 4.6. Latter consists of a lower and an upper part. The lower part looks very similar to the one used for EPR measurement. The upper part is a cap that's mounted on the Photocap. After the upper part has been positioned on the Photocap, the holding device is waterproof against the LED. Now the Photocap can be flooded with electrolyte. The cap contains a small recess for positioning the reference electrode (the reference electrode is then in the electrolyte bath during the measurement, but not directly above the Photocap). Holders can be adjusted in height and have an opening at the bottom. That's necessary that Photocaps can then be illuminated with the highest possible light intensity.
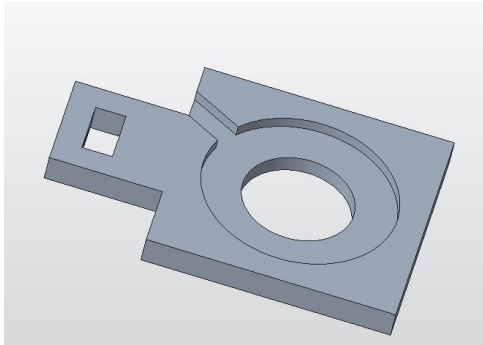
Figure 4.5.: Photocap holder for EPR measurements, with a lateral opening for contacting the back electrode
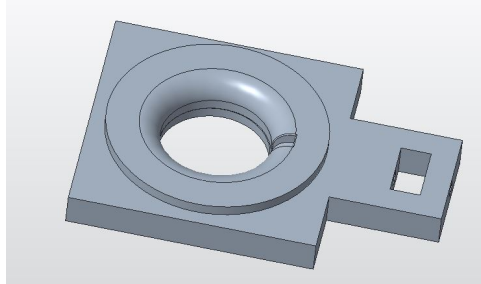
Figure 4.6.: Photocap holder for FP measurements, with cap to float the Photocap

4.1.2. EPR measurement

For the characterization of the EPR, measurements were carried out with different voltage amplitudes and pulse duration. Those parameters were set at a light controller which then illuminated the Photocap. Another additional factor, the drop size, was always tried to keep equal (with a standard drop size which has a diameter of about 2 mm to 3 mm). The distance between the measuring electrode and the Photocap could unfortunately not be measured, but again attempts have been made to keep the distance as small as possible, in order to obtain better measuring results (higher voltage values). For better clarity, the results have been summarised here. A list of all the measurement series can be found in the Appendix in Chapter 6. The mode of operation of a Photocap can be seen in fig. 4.7 by comparing the set pulse and pause duration on the light controller with the actual on and off time of the excited Photocap. Furthermore, a transient decreasing course of the measured voltage peaks can be seen here, which will be examined in more detail in the following section.
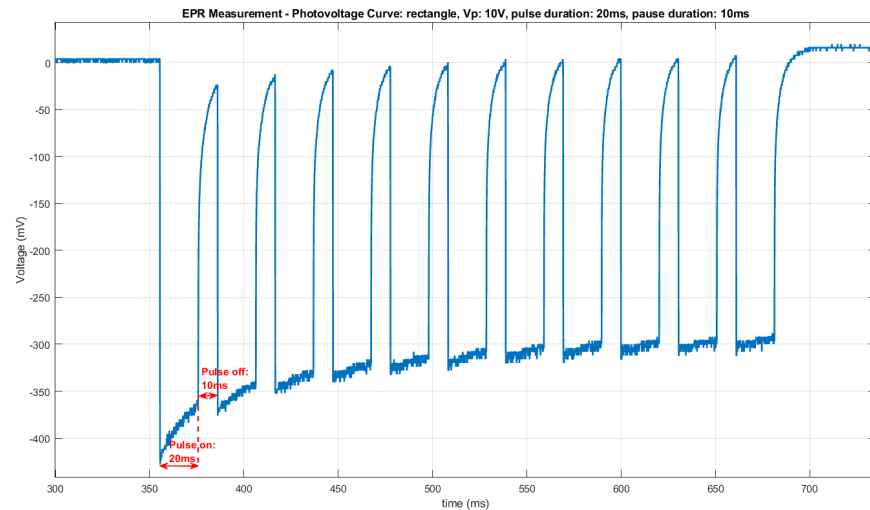
Figure 4.7.: EPR Measurement: Rectangle pulse with a voltage peak of 10 V, pulse duration: 20 ms, pause duration: 10 ms

Photocap charging behavior

During the EPR measurements it could be seen that the Photocaps showed a very distinct capacitive behaviour. The devices charged very quickly after a light pulse was emitted and took then a very long time to discharge. This behavior was investigated in more detail and is now described in this section.

In order to characterize the charging behavior of a Photocap more closely and to find out how long a pause for a light pulse should be, the device was illuminated at the beginning with a 20 ms pulse followed by a 5 ms pause. After that the pause duration was increased step by step. Fig. 4.8 shows the light pause duration over the maximum voltage deviation (measured between max. and min. peaks). This graph demonstrates that, in a series of pulses as shown in fig. 4.7, a Photocap can only recharge to a maximum voltage value if the pause between the light pulses is large enough. Subsequently an approximate rule of thumb for pause length per pulse length was derived.
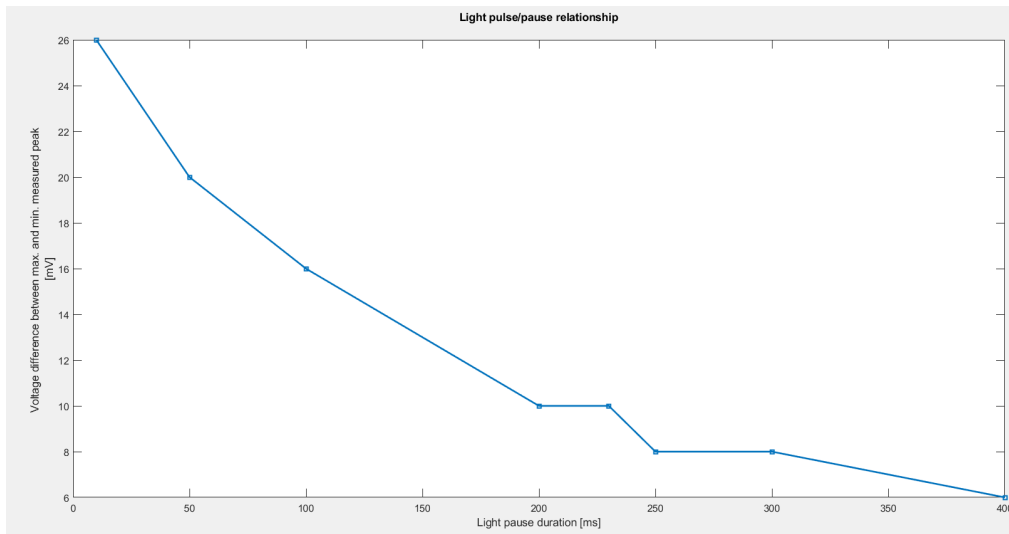
Figure 4.8.: Light pause duration for a 20 ms light pulse over the measured voltages difference (between maximum and minimum measured voltage peaks)

The plots of this step-by-step experiment can be taken from the appendix and serve as basis for eq. 4.1.

Rule of thumb for pulse/pause duration

$$\text{Pause duration for a } 1\,\text{ms pulse} = \frac{400\,\text{ms pause}}{20\,\text{ms pulse}} \approx 20\,\text{ms} \qquad (4.1)$$

Consequently, these results lead to the following consequences for the stimulation of cells.

Consequencess for cell measurements

The process of characterizing Photocaps has provided important results that help to better understand the charging and discharging behavior of such devices. Because of the ability to store charges in a very good way, it takes a rather long time till Photocaps discharge. As a result, it becomes **difficult to stimulate neurons** with such a charge behavior. Neurons want to be stimulated as short and intensive as possible. Here it is likely to happen that the discharge phase takes too long

and therefore neurons cannot be stimulated. In order to to the requirements of
3.3.2, it has to be mentioned at this point that if the charging behaviour of such an
optoelectronic device is to be fully exploited and operated efficiently, the stimulation
frequency must be relatively low. The optimal stimulation frequency is calculated
in eq. 4.2.

$$f_{Stim} = \frac{1}{T} = \frac{1}{1\,ms\,pulse + 20\,ms\,pause} = 47.62\,Hz \tag{4.2}$$

Light offset

A Photocap is a light sensitive device. Measurements in a Faraday cage were taken
with and without ambient and microscope light. The difference between these
two measurements with an offset of approx. 116 ms (with light) can be seen in the
following images.
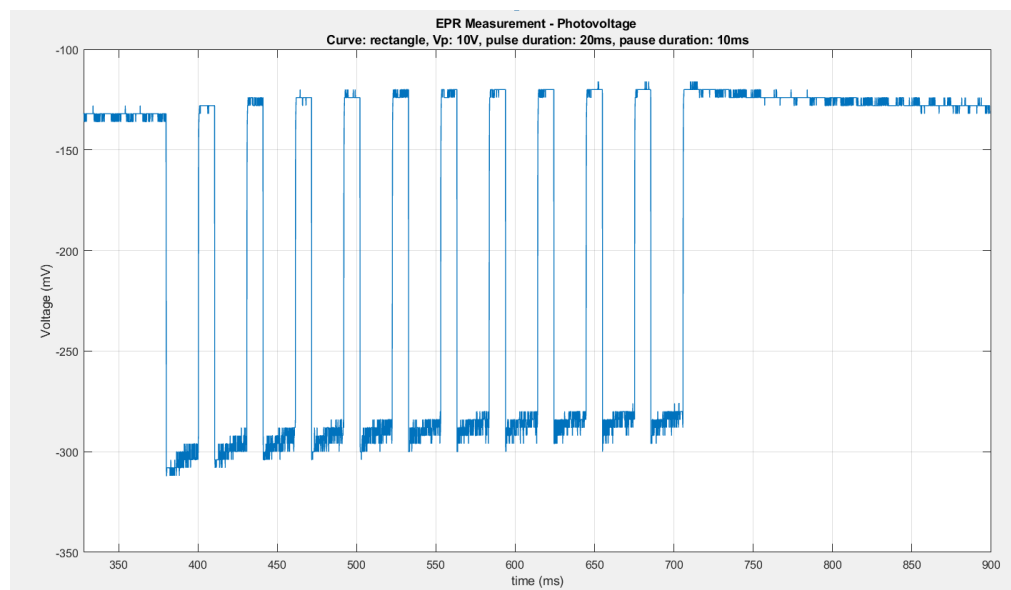
Figure 4.9.: EPR measurement with surrounding light
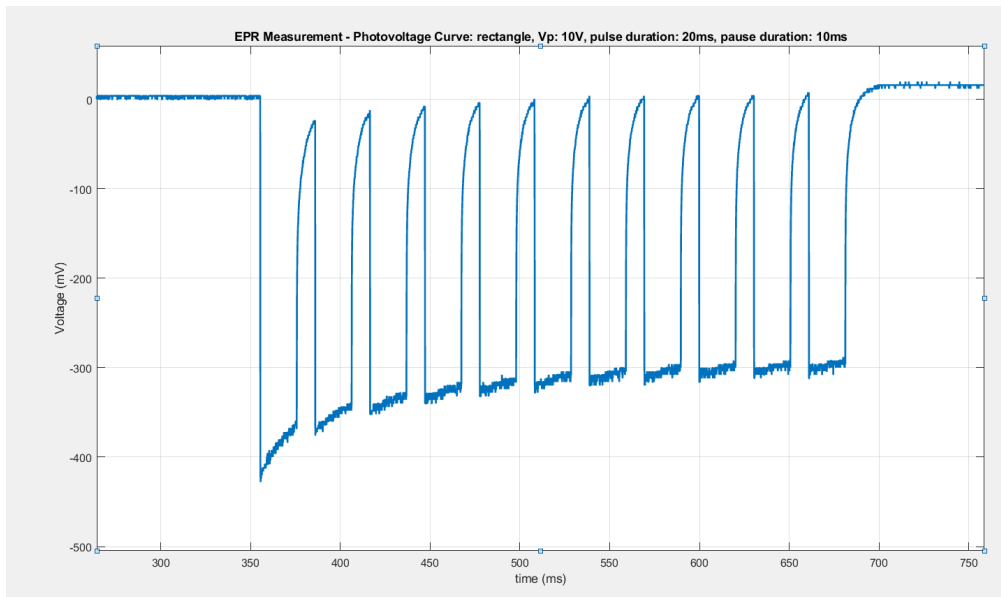
Figure 4.10.: EPR measurement without surrounding light

Measurements were always performed as dark as possible to keep the offset as small as possible.

4.1.3. Field potential measurement

During the field potential measurement, the voltage in the electrolytically conductive bath was measured between the pipette electrode and the reference electrode hanging in the bath. Measurements were taken at different positions of the measuring pipette: starting from the centre of the PN field where the highest voltage (of about -55 mV) could be measured. Followed by measurements at the edge of the PN field all the way to the outside of the PN field. Positions could only be set manually using a micromanipulator without knowing the exact x-y-z position. Photos were taken to interpret measured results according to the electrode position, examples are shown in 4.11 and 4.12.
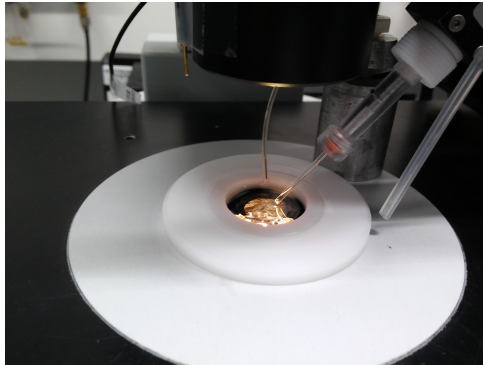
Figure 4.11.: FP measurement where the measuring pipette is in the centre of the PN field
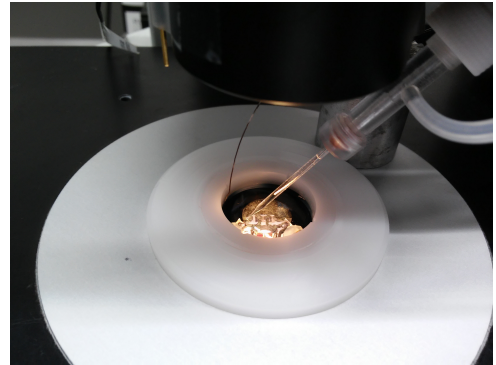
Figure 4.12.: FP measurement where the measuring pipette is at the left PN border

To characterize the distribution of the field potential, KCL (intracellular and extracellular) was used as in [21] and [9]. In this way, the results obtained, shown in 4.13, can be compared with those from previous publications, as it will be discussed later in Chapter 5. Measurements were also carried out with intra- (in the graduated pipette) and extracellular chicken solution (in the bath), as it will later be the case in practice with cell measurements. These measurement results are not discussed further in this thesis and can be found in the Appendix for the sake of completeness. The measured field distribution is displayed graphically in fig. 4.13.
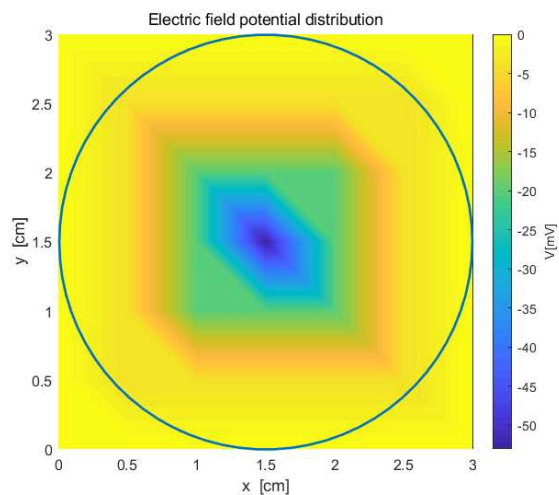
Figure 4.13.: Field potential results with a Photocap floated in a KCL bath

4.2. Equivalent circuit diagram

PSpice Schematics 9.1 was used for the simulation of electrical circuits. As described in Chapter 2.2.1, the simulation was split into several parts. The implementation and the simulation curves are described in the following sections.

4.2.1. EPR simulation

In the simulation part parameters were deliberately chosen in order to obtain same results as in practice of an EPR measurement. A separate simulation of such a measurement allowed to develop a better understanding of the mode of action of a Photocap. The equivalent circuit for an EPR measurement and the corresponding voltage curve are shown in 4.14 and 4.15. The model shown here was especially developed without consideration of [unit]/cm^2. The explicit recalculation (related to the drop size) and development of a model and specification of component parameters in [unit]/cm^2 is discussed in the next subsection.
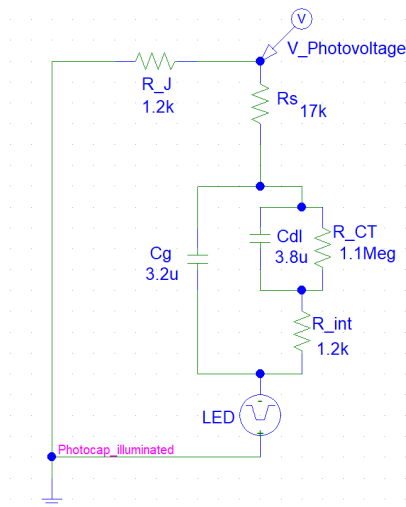
Figure 4.14.: EPR circuit without consideration of [unit]/cm^2
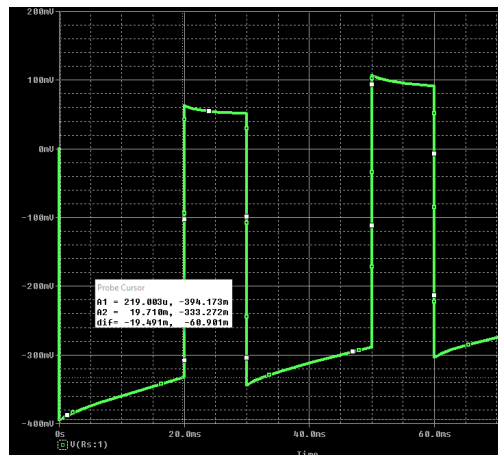
Figure 4.15.: EPR corresponding voltage curve without consideration of [unit]/cm^2, with 6 V set at the light controller

Size of parameters

As already described in section 3.2 the idea for the construction and in some cases the order of magnitude of the components comes from the EIS which was carried out with an earlier version of a Photocap[20]. While C_{dl} = 3.8 µF, R_{CT} = 1.1 MΩ and R_{int} = 1.2 kΩ were the same size as determined in the EIS, C_g = 3.2 µF was set to best fit the results. Rs describes the resistance of the electrode material and the electrolyte used (in this case a 3 M KCL drop) and was determined to be 17 kΩ. The junction-width resistance must be relatively large in a measurement where the junction is produced by only one drop. This was fixed with 1.2 kΩ instead of about 380 Ω originally specified in the Paper[24].

4.2.2. EPR expressed in [unit]/cm^2

Subsequently the drop size was taken into account in a electrical circuit, shown in 4.16 and fig. 4.17. The information is now expressed in [unit]/cm^2 and can theoretically be used for subsequent models, e.g. field simulations in FEM tools like it was used in [21].
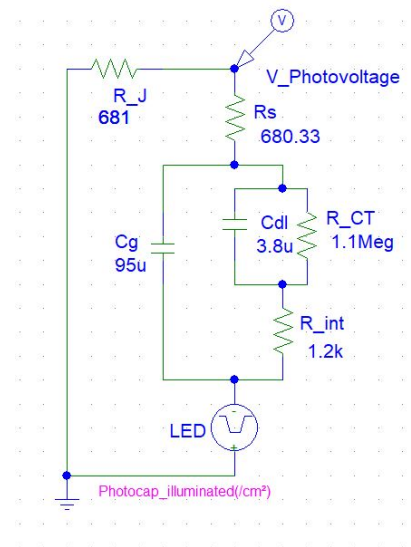
Figure 4.16.: EPR circuit with consideration of the droplet size
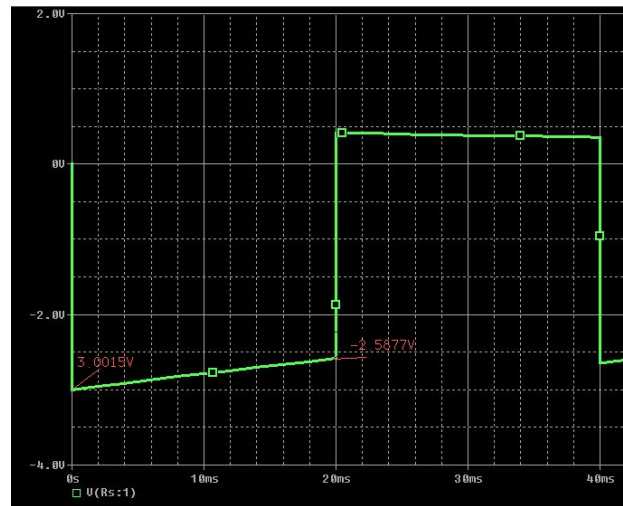
Figure 4.17.: EPR corresponding voltage curve, with 6 V set at the light controller

Consideration of drop size: 1 ml of liquid usually contains about 20 drops. One drop has a diameter of about 2.5 mm. Since in this work EPR measurements were usually performed with one drop of a standard length of 2.5 mm, it follows:

$$1\text{drop} = \frac{1\,\text{ml}}{20\,\text{drops}} = 50\,\mu\text{l} \tag{4.3}$$

The calculation was based on a mean value of -412.57 mV (measured photovoltage peaks in a range of 4.5 V to 10 V set at the light controller). Since KCL has a conductivity of about 300 mS/cm and 1 droplet has about 50 μl, by transforming the liquid volume into cm^2 it results in 0.1357 cm^2:

$$\frac{-412.57\,\text{mV}}{0.1357\,\text{cm}^2} = -3.04\,\text{V/cm}^2 \tag{4.4}$$

Size of parameters expressed in [unit]/cm^2

As in the previous simulation, [20] again delivered ideas for an initial sizing of components. Since a parametrization on a [unit]/cm^2 level should take place, the order of magnitude of the components had to be considered in a right way.

While $C_{dl} = 3.8\,\mu\text{F}$, $R_{CT} = 1.1\,\text{M}\Omega$ and $R_{int} = 1.2\,\text{k}\Omega$ again were the same size as determined in the EIS, $C_g = 95\,\mu\text{F}$ was set to best fit the results. The order of magnitude for Rs was based on [25]. In this research an EIS with ITO+PEDOT:PSS was performed and a size of 667 Ω was determined for Rs.

Furthermore, the standard drop size had to be considered:

- 3 M KCL = 300 mS/cm
- 1 drop with a standard drop-length of about 2.5 mm

...which than leads to a resistance of:

$$\frac{2.5\,\text{cm}}{10} * \frac{300\,\text{mS}}{\text{cm}} = 75\,\text{mS} = 13.33\,\Omega \tag{4.5}$$

This results in

$$\text{Rs} = 667\,\Omega(\text{ITO} + \text{PEDOT} : \text{PSS}) + 13.33\,\Omega = 680.33\,\Omega \tag{4.6}$$

R_J was then fixed with a size of 681 Ω.

4.2.3. Field potential simulation

The bath solution was taken into account in the equivalent circuit, shown in 4.18 and fig. 4.19. Orders of magnitude are expressed in [unit]/cm². The expression in [unit]/cm² is necessary to allow an interaction between the equivalent circuit diagrams and the action potential simulation model for different cell sizes.
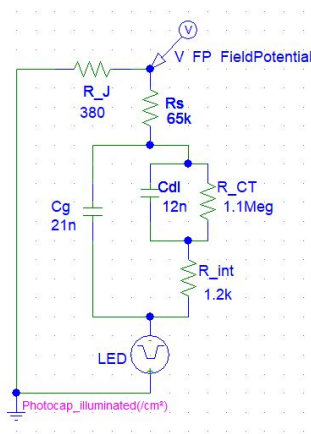

Figure 4.18.: Electrical field potential circuit with consideration of the filling level in a bath and expression in [unit]/cm²
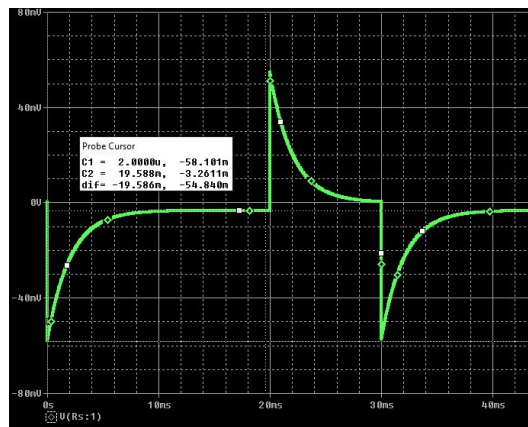
Figure 4.19.: Corresponding voltage curve with consideration of [unit]/cm²

Size of parameters

In the field potential simulation, the following parameters were left at pre-defined values (see [24] and [20]):

- R_J = 380 Ω
- R_{CT} = 1.1 MΩ
- R_{int} = 1.2 kΩ

Rs has, in comparison to the two previous simulations, the largest value of 65 kΩ, since the current here has to overcome a large resistance by the filled bath. C_{dl} and C_g have also been modified accordingly to ensure that the simulation results correspond to the measurement results obtained in practice, taking into account the filling level in the bath.

Consideration of bath solution: The field potential measurement was usually performed with a filling volume of 1 ml. 1ml contains approx. 20 drops. We already know that 1 drop has about 50 µl and that 1 ml corresponds to 1 cm^2. Therefore the electric field potential voltage in the model has to look as follows:

$$\frac{V_{FP_{max}}}{1\,\text{ml}} = \frac{-55\,\text{mV}}{1\,\text{cm}^2} \tag{4.7}$$

The calculation was based on the maximum measured value of with $V_{FP_{max}}$ = -55 mV (measured centrically of the PN field at approx. cell height)

4.2.4. Entire equivalent circuit model

A comprehensive simulation of the whole measurement setup can be seen in fig. 4.20 below. The illuminated Photocap simulation part is taken from the field potential simulation in 4.2.3, with a modified Rs, since the distance between cell and Photocap and thus the electrolyte distance is in the nm range, as described in [24]. The cell simulation part is based on the ideas of [24], already described in Chapter 3.2 and consists of two facing Luo-Rudy-Ebihara-Johnson cell models. The lower part represents an attached cell membrane, while the upper part represents the free cell membrane. The Patch Clamp part has been omitted for simplicity's sake, as it doesn't matter at this point, since we are primarily interested in the

membrane potential. It becomes important for the subsequent process, when cells have to be clamped to a certain potential.
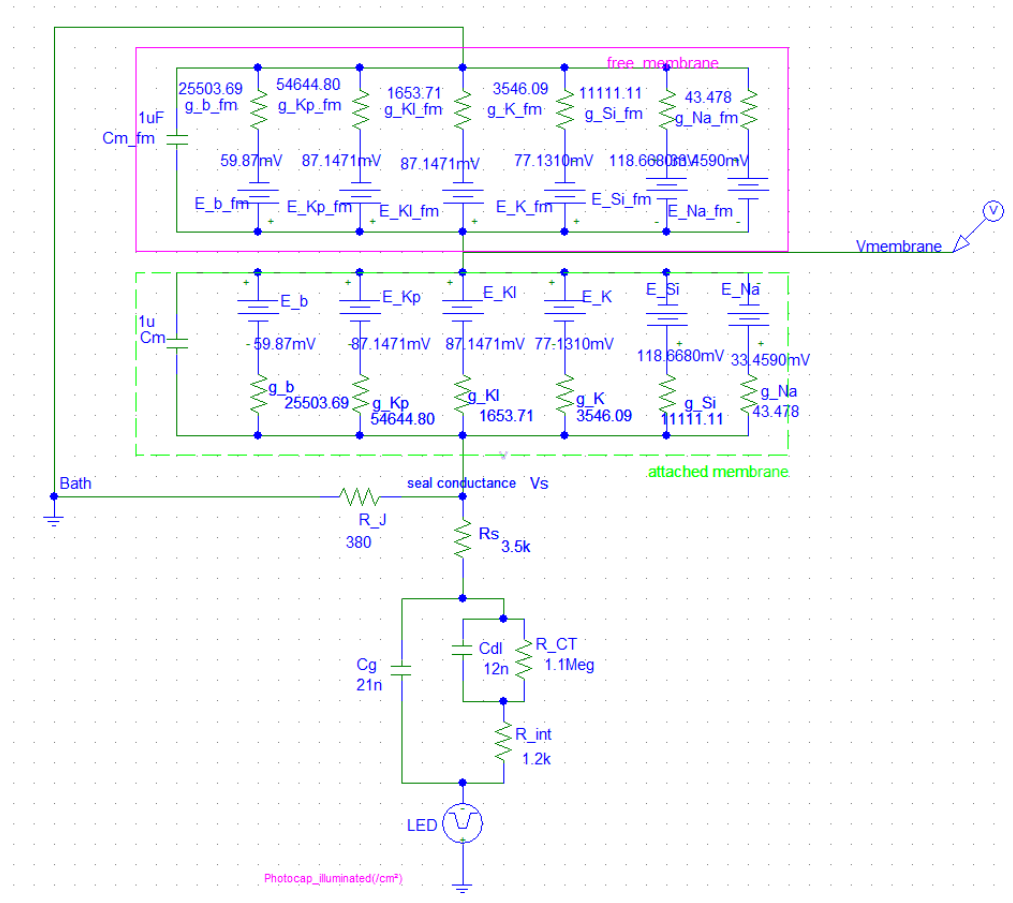
Figure 4.20.: Equivalent circuit diagram of the total Photocap-cell-measurement Setup in PSpice

Since such a model does not yet exist, the equivalent circuit model was deliberately kept simple in order to develop a better understanding of the mode of action. This means that the time and voltage-dependent slow inward current and potassium channel (Kp) were kept simple at their initial values, as the maximum excursions of the voltage curve following the stimulus were of primary interest. Apart from that, the course of slow inward current, the potassium and the changing calcium can be analyzed in more detail in the Matlab model. The calcium concentration,

the reverse potential of slow inward current and slow inward current dependencies can be seen in the following formulas eq. 4.8, eq. 4.9 and eq. 4.10 below.

$$\frac{dCa_i}{dt} = -10^{-4} \cdot I_{si} + 0.07 \cdot (10^{-4} - [Ca]_i) \tag{4.8}$$

$$E_{si} = 7.7 - 13.0287 \cdot \log([Ca_i]) \tag{4.9}$$

$$I_{si} = g_{Si} \cdot d \cdot f \cdot (V_m - E_{si}) \tag{4.10}$$

4.3. Action potential simulation of excitable cells

Matlab version **R2018a (9.4.0.813654)** and **R2019b (9.7.0.1190202)** were used for the implementation of a cell model for the simulation of action potentials. In this chapter the achieved plots of the implemented model are presented.

While fig. 4.21 represents a triggered action potential for a monophasic rectangular current pulse, the obtained plot 4.22 was achieved by stimulating the virtual cell in the Matlab model with the stimulation current (derived from the resulting maximum field potential voltage from the equivalent cell model). Further details have already been described in Chapter 3.

Action potential with Time step:0.01
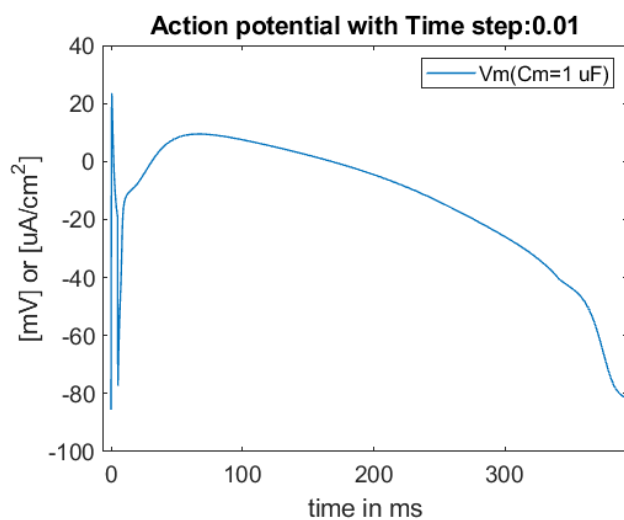
Figure 4.22.: Action potential triggered by a biphasic current pulse (derived from the maximum measured field potential voltage)

Action potential with Time step:0.01
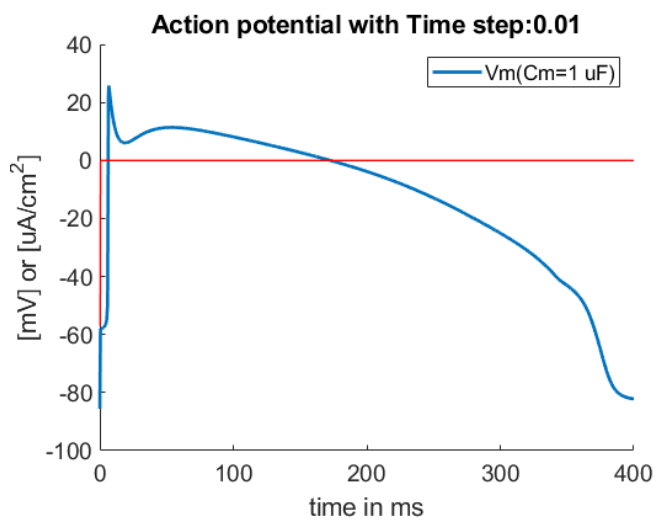
Figure 4.21.: Action potential triggered by a monophasic 5ms rectangular pulse

The current curve shown below in fig. 4.23 was derived from the maximum field potential voltage curve shown in fig. 4.24 after time. It corresponds to the voltage curve measured in the simulation of the field potential, shown in 4.19.
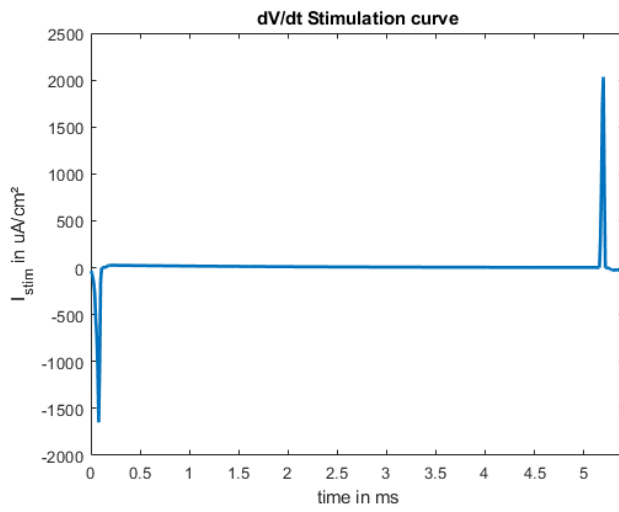
Figure 4.23.: Derived voltage curve: $I_{stim} = dV/dt \cdot Cm$
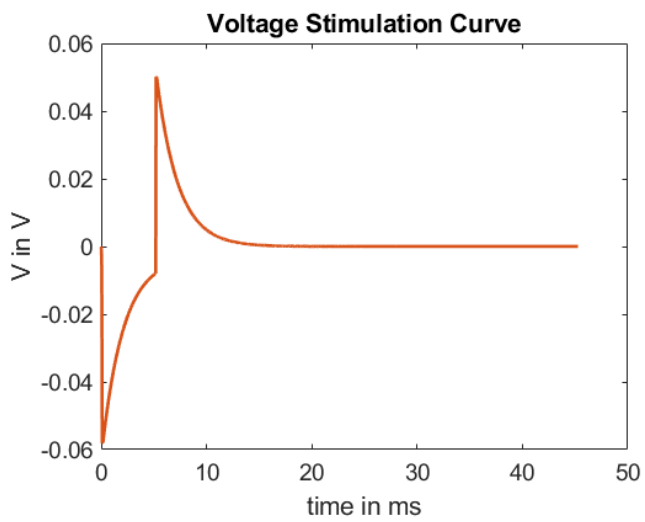
Figure 4.24.: Measured field potential curve out of equivalent circuit simulation

4. Results

Strength-duration curve

In this section the measured strength duration curve for a Luo-Rudy-Ebihara-Johnson is presented. Fig. 4.25 shows the stimulation duration over the min. current which is able to elicit an action potential
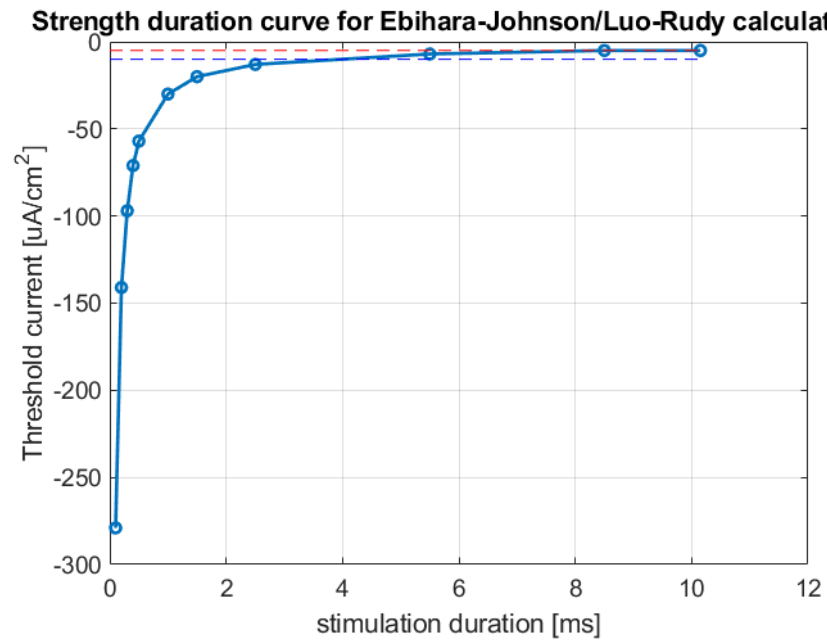
Figure 4.25.: Strength duration curve for a Luo-Rudy-Ebihara-Johnson implementation

Threshold voltage

Voltage-controlled ion channels will be activated at the threshold-voltage. For the above shown SD-Current the threshold voltage shown in fig 4.26 lies at approx. $-57.5\,\mathrm{mV}$.
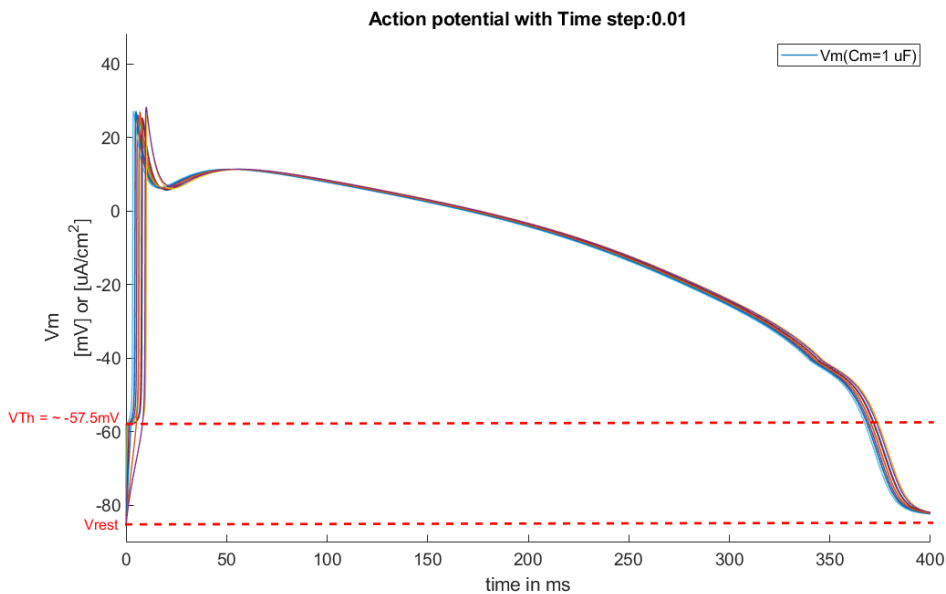
Figure 4.26.: Threshold voltage at about $-57.5\,\mathrm{mV}$

4.4. Chicken cardiomyocyte measurements

Parameters from practice could not be provided yet, because Patch Clamp measurements at the Medical University of Graz could not achieve successful results so far. Improvements and solutions are under development.

5. Discussion

The aim of this work was to find out whether excitable cells in an external electric field, generated by an illuminated Photocap, can trigger an action potential. To find this out, it was necessary to develop a model that made it possible to simulate individual measurements up to the entire measurement setup. Subsequently, it was also necessary to implement a mathematical model that enabled the simulation of the action potential of excitable heart cells.

Originally, it was planned to develop a simulation model for excitable nerve and heart cells. The signals generated in the model should then be compared with those obtained in practice (i.e. with measurement results on real cells). However, since the measurements in reality turned out to be more difficult than expected, it was decided to focus initially on chicken cardiomyocytes. These cells are easier to handle especially at the beginning, because when an action potential is triggered it lasts longer than an action potential of a nerve cell would. In addition, there is a strong expertise at the medical university in the field of heart cell measurement. However, a Hodgkin-Huxley model has already been implemented which can be extended and adapted at any time [30]. The basis of the equivalent circuit (EPR simulation and field potential simulation) can be used for both excitable cell types, only the electrical circuitry for the cell model has to be adapted to the ion channels and gate mechanisms for nerve cells.

5.1. Comparisons of achieved versus researched results

This chapter compares the differences between the measurement results obtained to those in the literature. Essential differences are largely based on the fact that in this thesis we are dealing with a new, still partly unexplored, technology.

5. Discussion

5.1.1. Comparison of measured Photovoltages

The obtained results of the EPR measurement can be found in Chapter 4.1.2. In the two pictures below (fig. 5.1 and fig. 5.2) the measured photovoltage from the EPR measurement can be compared with the one of the Swedish research team[8]. At first sight it can be seen that the measured photovoltage in the left image is larger than the one in the right. However, this can be due to several reasons. The main reason is probably that the measured photovoltage in the right image was measured with a Photocap without PEDOT:PSS, while in the left image it was already measured with a Photocap with PEDOT:PSS, which improves the capacitance of the Photocap as described in Chapter 1.3. Furthermore, in the measured photovoltage curves of the EPR measurement it can be seen that Photocaps have the ability to work very accurately, i.e. the controller settings (light pulse on and light pulse off) were converted by the Photocap almost without delay. As mentioned in Chapter 4.1.2, the characterization of Photocaps showed a very good charge-storage behavior, which means that a Photocap takes a relatively long time to discharge. This behavior could also be reproduced in the simulation.
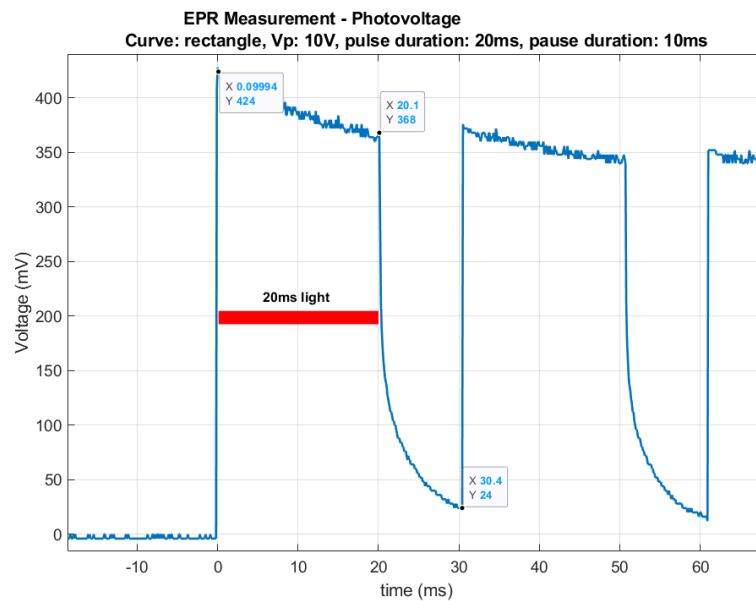
Figure 5.1.: Measured photovoltage in an EPR Measurement

Figure 5.2.: Photovoltage measured in [20]

5.1.2. Comparison of ramp and rectangular stimulation in simulation

As discussed in Chapter 1.2.2, it was decided to control the Photocap with a rectangular light pulse, since this allows higher voltage peaks. This was checked in the generated simulation model both for the EPR measurement and in the electric field potential simulation. In both simulations higher voltage values could be achieved with square-wave pulses than with ramp-wave pulses, which proves the statement in [8]. Fig. 5.3 shows an EPR simulation in which a Photocap is excited by a square pulse. The measured peak of about $-371\,\text{mV}$ is greater than in fig. 5.4 , where the Photocap with the same applied voltage peak but ramp stimulation can only reach a lower voltage of about $-362\,\text{mV}$.

5. Discussion
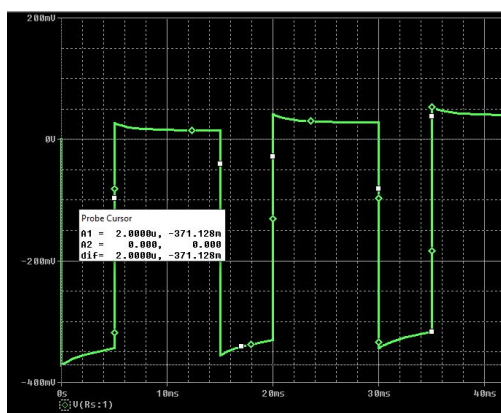
Figure 5.3.: Electrical photoresponse simulation with a 5 ms rectangular pulse
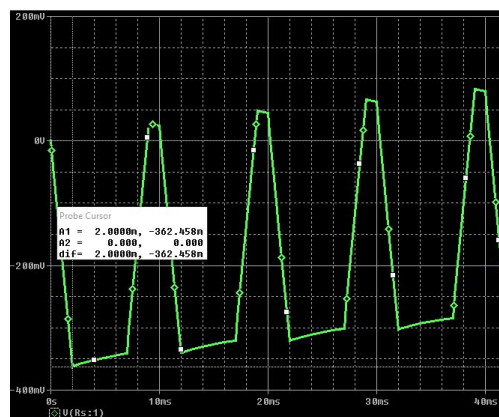
Figure 5.4.: Electrical photoresponse simulation with a 5 ms ramp pulse

The same as for the EPR was also tested in the electrical field potential simulation. While with a square wave pulse approx. $-58\,\text{mV}$ could be measured, with a ramp stimulation only about $-38\,\text{mV}$ could be achieved, shown in fig. 5.5 and fig. 5.6.

Figure 5.5.: Electric field potential simulation with a 5 ms rectangular pulse

Figure 5.6.: Electric field potential simulation with a 5 ms ramp pulse

5.1.3. Comparison of measured electric field potentials

The obtained field potential measurement results can be found in Chapter 4.1.3. While fig. 4.13 shows the measured distribution of the electric field potential which propagates over a Photoc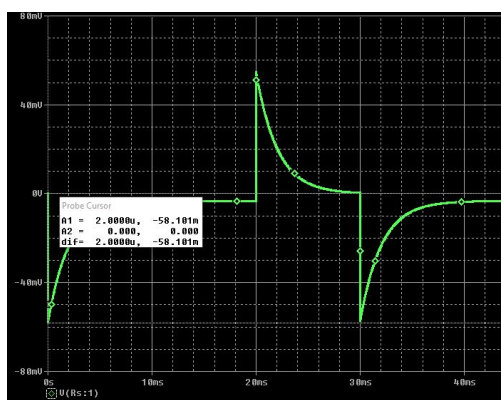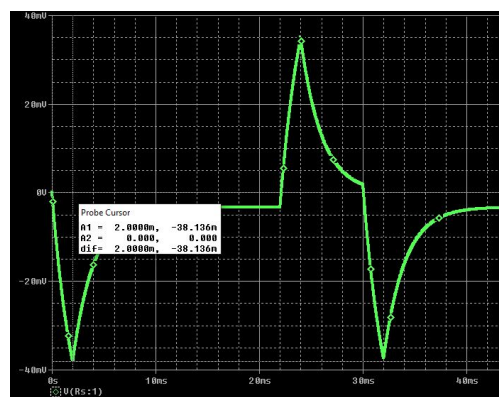ap in an electrolytically conductive bath, fig. 1.14 refers to the result shown in [21]. An interesting discovery is that the measured maximum peak in fig. 4.13 (about $-55\,\text{mV}$) exceeds the peak in fig. 1.14 (about $-40\,\text{mV}$).

The measurements of the electrical field distribution in a bath turned out to be very difficult in practice, since such a measurement is an interplay of many small factors, some of them hardly influenceable. Some of these factors are:

- Length of the glass pipette (were newly manufactured for each measuring cycle, not always identical)
- Filling level in the glass pipette
- Filling level in the bath

Since the micromanipulator can only be controlled manually, no absolute agreement between different measurements could be guaranteed for the following factors:

- Distance between measurement pipette and Photocap
- X-Y position of the measurement pipette

Furthermore, inexplicable noise often occurred at one of the two measuring stands available at the Medical University of Graz for measuring the electrical field distribution. The sensitive measuring stand used was the one surrounded by a Faraday cage. Probably there was an undefinable source of interference in the cage, which had a big influence on the measurement results. In addition, the light controller was not working completely error-free above $6\,\text{V}$, which often led to oscillations in the measurement signal. Such a behaviour for the maximum measured voltage is shown in 5.11. However, this had no influence on the maximum measurable voltage.

It can be said that achieved measurement results nevertheless exceeded expectations, though the way to reach these results was very challenging and time consuming.

5.1.4. Comparison of action potential simulation curves

Below, the curves generated in the Matlab model are compared with those of the research on Isolated Chick heart cells [26]. At this point it is important to mention that the cited research paper should only serve as a basis for the implementation of the Matlab model. The aim has never been to achieve exactly the same results, but only to generate the most suitable model for modeling chicken cardiomyocytes. This means that the deviation of the curves shown below is largely due to the different stimulation current. In both cases a biphasic stimulation was used. The curves in the left illustrations can be compared with the dashed curves in the right diagrams.
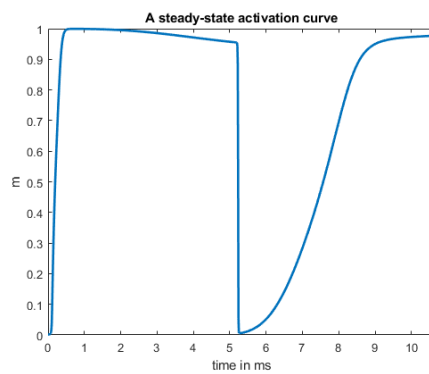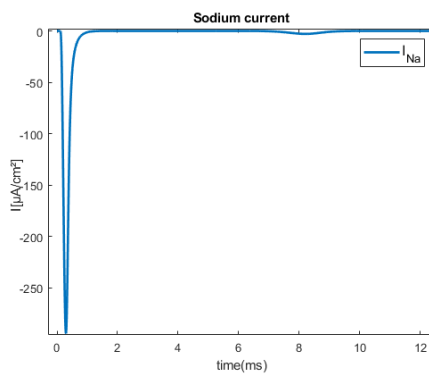
Figure 5.7.: LREJ m gate

Figure 5.8.: m gate with reference to [26]

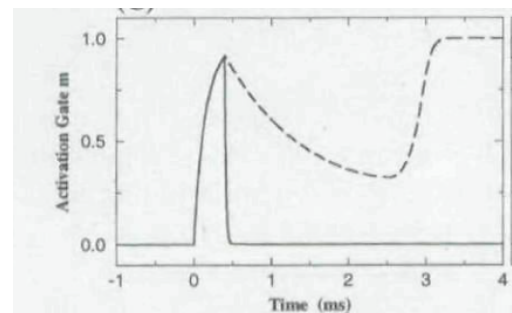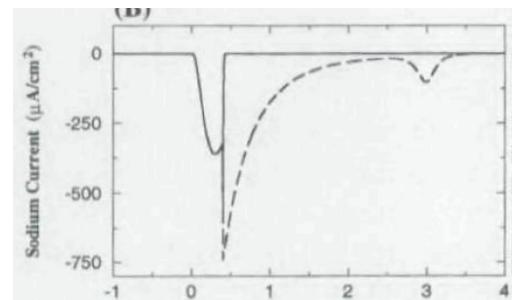Figure 5.9.: LREJ fast sodium current I_{Na}

Figure 5.10.: I_{Na} gate with reference to [26]

5.1.5. Comparison with chicken cell measurements in practice

The main idea, to develop a model for excitable heart and nerve cells, had to be abandoned because the measurements in practice, with which the model should be compared in the end, turned out to be difficult. Unfortunately, cells were unwilling to grow on the Photocaps, which then turned out to be difficult to stimulate chicken cells. Furthermore, the measurement setup has been a problem so far: The microscope is needed to puncture cells with the measuring pipette. The LED controller needed to excite the Photocap and the microscope cannot be used at the same time. Since cells contract spontaneously and pipettes jump out of the cell membrane, it is a problem to switch between using the LED controller and the microscope needed for patching. However, improvements are already being made, e.g. coating of the Photocaps, improvements to the measurement setup, etc..

5.2. Equivalent circuit

I decided to split the equivalent circuit into several parts to get a better understanding on how Photocaps work in different situations. The simulation of EPR measurements (with and without consideration of $[unit]/cm^2$) and the simulation of field potential measurements could be implemented successfully as equivalent circuits.

Nevertheless, a model could be implemented to get an idea how big the voltage (or current) is that reaches the cell.

5.2.1. Comparison of the measured electric field potential

In fig. 5.11 the signal curve of the electric field potential measurement in an electrolytically conductive bath can be seen, showing the maximum measured value of -55.85 mV, with a set voltage value at the light controller of 10 V. The oscillation after the voltage peak in the signal comes from a malfunctioning of the light controller. Unfortunately the light controller did not always work properly over 6 V. But the oscillation has no influence on the measured maximum value. The measured maximum peak and the -9.85 mV after the transient course could

be reproduced quite well in a simulation, for comparison see fig. 4.19, where the maximum simulated voltage peak is $-58.1\,\text{mV}$
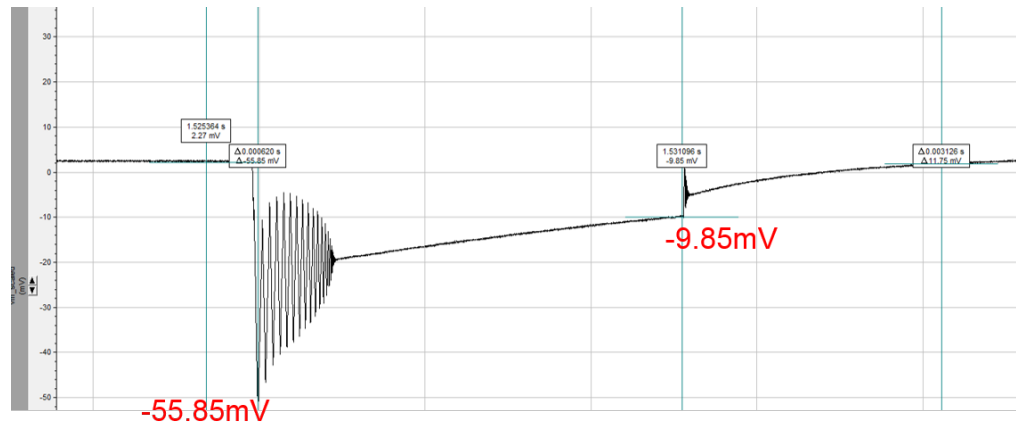
Figure 5.11.: FP measurement result, measured in a 3 M KCL bath

5.2.2. Equivalent circuit model versus Matlab model

This chapter shows the similarity between the plots generated by the electrical equivalent circuit and the plots generated in the cell model in Matlab. The equivalent circuit, as already described in Chapter 4.2.4 was deliberately kept simple initially, which means that the time and voltage dependence of the slow inward current and potassium (Kp) channel was deliberately ignored. In the model the reaction of the membrane voltage measured between the attached and free membrane following a 5ms light stimulus is shown. Fig. 5.12 shows the response of a specific biphasic stimulus in the Matlab model (which also takes into account voltage- and time-dependencies). Fig. 5.13 on the other hand shows the membrane voltage measured in the equivalent circuit after the same 5 ms light pulse.
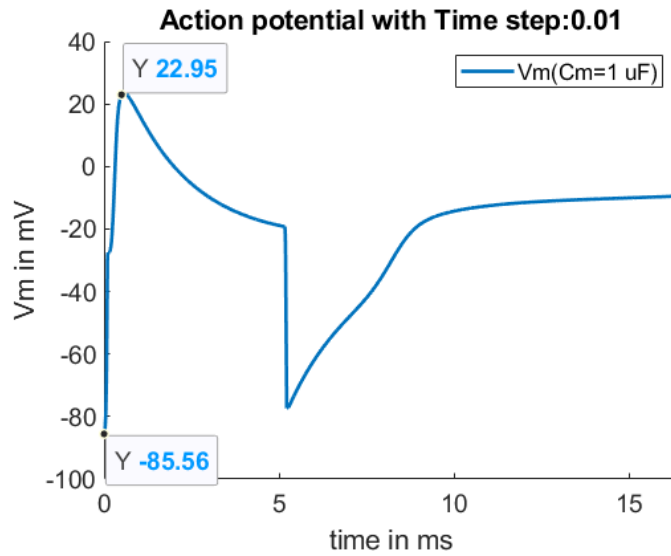
Figure 5.12.: Initial phase of an action potential after a biphasic stimulus

The minimum and maximum values of the membrane potential are -85.442 mV and 25.665 mV and thus correspond well with the minimum and maximum values in the Matlab model, namely: -85.56 mV and 23.55 mV. The attached cell membrane depolarizes according to the stimulus.
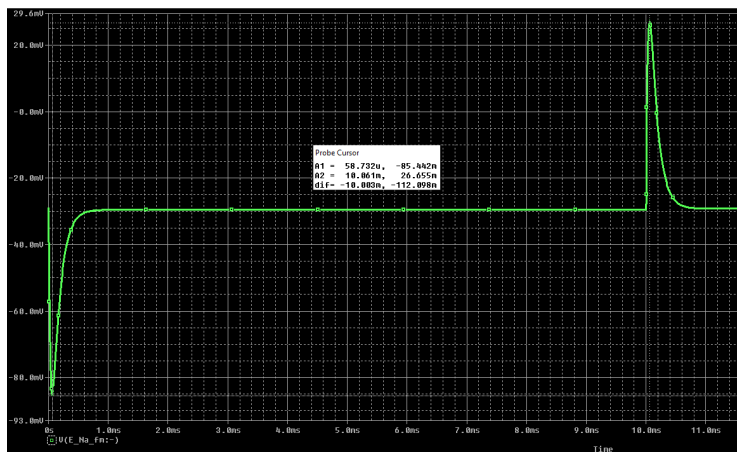
Figure 5.13.: Attached and free cell membrane voltage characteristic

5.3. Applying another use case to the simulation model

In addition to the first application, namely whether cells can be stimulated at approx. cell height in the centre of the PN field, triggering an AP was successfully shown. In a further application case it should now be determined whether it is theoretically possible to trigger an action potential when cells are growing at the edge of the PN field.

From the practical measurement results of the field potential measurement shown in fig. 4.13, we know that at the edge of the PN field (at approximately cell height) the field potential voltage has a voltage of approximately -26mV. Since this is a tricky example, the threshold and SD curves can here be used as an aid to solve this issue. Fig. 4.26 showing the threshold voltage at about $-57.5\,\text{mV}$ and fig. 4.25 showing the SD curve. From the SD curve we know that a stimulation pulse for currents $<-50\,\mu\text{A}/\text{cm}^2$ should be as as short as possible, means approx. 0.1 ms.

Starting this application with the measured field potential voltage of about $-27\,\text{mV}$, shown in 5.14.
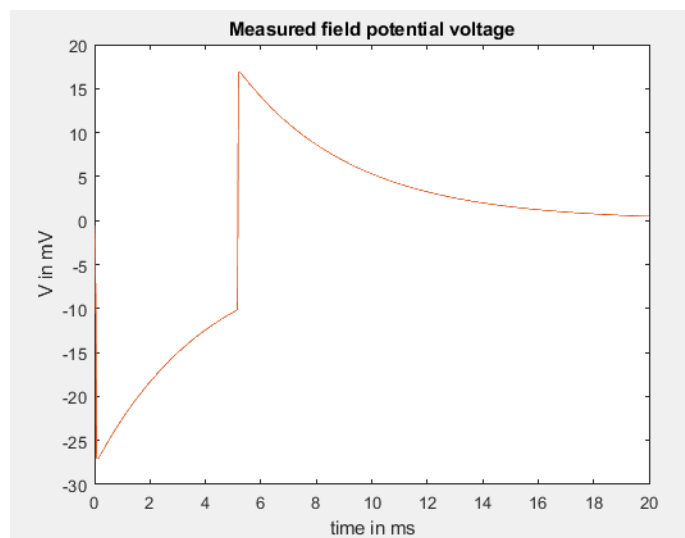
Figure 5.14.: Measured field potential voltage at the PN border

This field potential voltage was then derived after time to obtain the stimulation

current, which was then sent to the virtual cell model. The stimulation current with a magnitude of $-784.8\,\mu A/cm^2$ is shown in fig. 5.15.
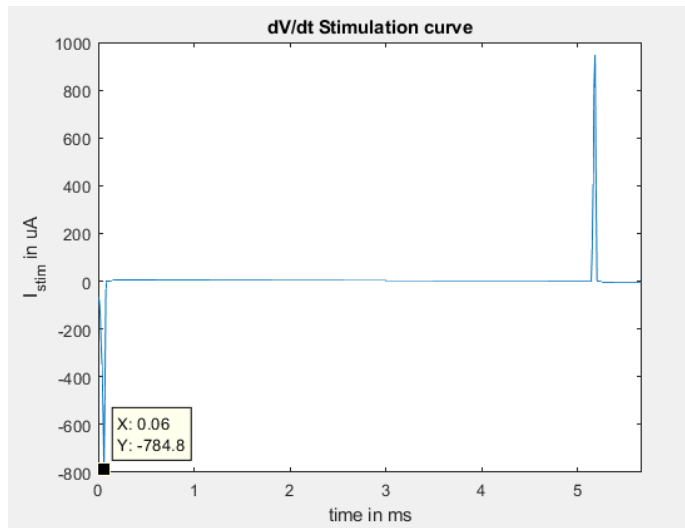
Figure 5.15.: dV/dt stimulation current

The answer of the cell in the model was then as follows, shown in fig. 5.16. No action potential could be triggered.
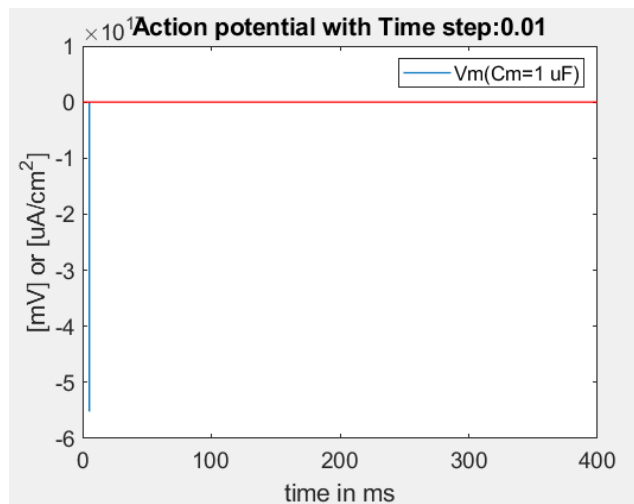
Figure 5.16.: Answer to the stimulation current of the cell model

69

5. Discussion

Now let's recalculate if it should theoretically possible to trigger an AP. The mixed model of LREJ has a threshold voltage of -57.5 mV. The resting membrane potential of the cell is about -85 mV, this means:

$$-57.5\,\text{mV(threshold voltage)} + 85\text{mV(resting membrane potential)} = 27.5\,\text{mV}$$

(5.1)

 that 27.5 mV have to be passed to trigger an action potential. Theoretically it should be possible to successful stimulate the virtual with this biphasic impulse, from figure 5.15.

We are dealing with nonlinear capacitive stimulation currents in practice, but the implemented model provides linear biphasic currents. We know from Chapter 1.2.2 that nonlinearities often play an important role in biphasic currents, thus we now want to make the linear biphasic current less linear. That should be done by making the negative flank slightly longer than the positive flank, but the total pulse length remains the same than before. The negative flank now takes 0.07 ms while the positive flank lasts for 0.03 ms instead of 0.05 ms-0.05 ms we had before. The result of the virtual cell model then looks as follows:
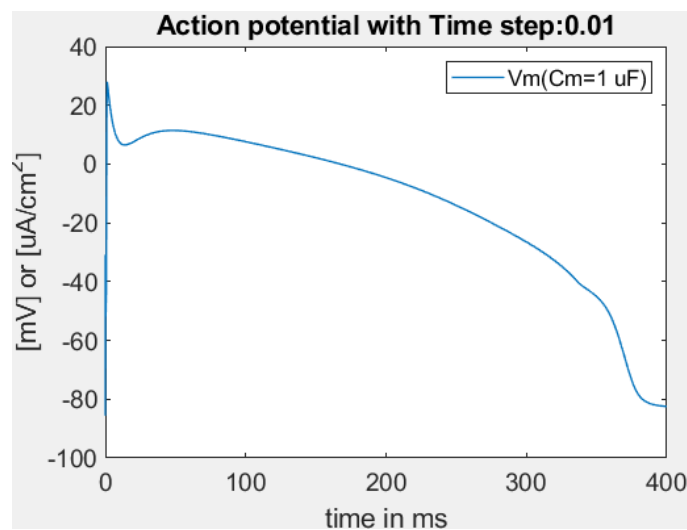
Figure 5.17.: Answer to the stimulation current of the cell model

By adding non-linearities to the biphasic pulse, but having the same total duration than before, an action potential could be triggered.

Conclusion: This use case shown here proves one big difference between monophasic and biphasic pulses. For large stimulus pulses the two stimulation types react very similar, since the entire pulse-duration is equal, e.g. 10 ms(monophasic) and 5 ms/5 ms pulse. But in some cases, the non-linearity in biphasic pulses play an important role. Otherwise it may be possible to not trigger an AP, as it was shown in this use case.

In summary, it can be said that the nonlinearity of the biphasic pulse plays an important role for theoretical very short pulses. Since this thesis deals with capacitive stimulation currents and therefore with non-linear stimulation currents, this is a great advantage for cell stimulation. Finally, it could be shown that action potentials in cells can also be triggered at the edge of the PN field.

5.4. What is the problem with Photocaps?

In practice, the characterization of Photocaps turned out to be difficult. Measuring systems could not be constructed one hundred percent identically and it lasted often longer until meaningful signals could be generated. In addition, much time passed until the first Photocaps were available for practical measurements. Furthermore PEDOT:PSS on the Photocaps had its own life. The staff of the Medical University, who already dealt with Photocaps before, recommended to let the Photocaps react in 3 M KCL, because then the effectiveness of the PEDOT:PSS would be better. Unfortunately, in one of two Photocaps, the entire PEDOT:PSS was removed. In addition, it turned out that the PN layer of these devices is very sensitive and starts to peel off at the slightest touch.

As already mentioned in 5.1.3, there is a range of factors involved, which make it hard to perform identical measurement results. A number of factors and questions that need to be considered before measurements are taken are listed below.

- Positioning of the measuring pipette (x,y-position, distance between Photocap and pipette)
- Droplet size (in the EPR measurement)
- Pipette quality
- Is the PEDOT:PSS even?
- Is the PN layer of the Photocap possibly scratched?
- Does the KCL already start to crystallize?
- Is the pipette clogged due to KCL crystallization?
- Has the test bench been darkened?
- Have all interferences been removed from the Faraday cage?
- Have mobile devices been switched to flight mode directly next to the test setup?

A very important point that emerged from this work concerns the loading and unloading behaviour of Photocaps. While the long charging time is advantageous for heart cells, it could mean a big disadvantage for nerve cells, because they like to be stimulated for a short time. It will become difficult to stimulate neurons with such a long charge behavior, since Neurons want to be stimulated as short as possible, which would then violate with one of the basic statements of this project. On the whole, first successful measurement results and simulation results were achieved. Due to the cooperation in this project between TU Graz and Medical University of Graz several new solutions could already be developed and considered. We benefit from the mutual knowledge and willingness to work on common solutions.

6. Conclusion

In the context of this master thesis, the main question, namely whether cells can be stimulated by external stimulation using a Photocap, could be successfully answered.

In order to counteract the problem of reproducible measurements with regard to the factors that are difficult to influence, approaches to solutions are already being worked on.

The vision is...to develop an automated test system. The idea is to prepare only the Photocaps (before the measurement) and the measuring pipette, but not to position the measuring electrode. After entering the desired data in an input field, the system automatically moves to the requested position. Various measurement protocols should also be available at the beginning.

A reproducible EPR measurement depends not only on the constant distance between the measuring pipette and the Photocap but also on the droplet size. The measurements are more accurate the smaller the droplets are. This is exactly the problem, since no pipette was available that could provide such small droplets such as those required for this type of measurement. For this reason, an alternative solution has been worked out together with a bachelor student, specifically the use of the very precise syringe pump, shown in 6.1. The syringe pump is currently able to deliver drops in the range of $2\,\mu l$ to $4\,\mu l$. Currently, suitable glass pipettes are still being looked for that can deliver this exact drop size. In addition, factors like the angle of the measuring electrode, the concentration of the electrolyte used, alternative LEDs with lower power but more focused bundled light will be investigated in more detail.

Figure 6.1.: Syringe pump for a controlled drop delivery

A simulation goal for the future would be to include the calculation of the distribution of a non-homogeneous electric field. Currently, the electric field has been measured and is simulated with the maximum value that would be achieved by measuring at cell height in the middle of the PN field. Furthermore, the electrical distribution within the cell membrane, which has already been considered in this work but not detailed yet, should also be taken into account. Initial ideas on how such projects can be implemented have already been provided, e.g. by calculating the field distribution with the Laplace function and suitable boundary conditions.

> **The vision is...**to provide a complete unit of simulation that unifies both the equivalent circuit and the mathematical action potential simulation in one tool. The idea would be to identify all relevant factors at the beginning in order to achieve a meaningful simulation result; factors such as cell size, cell shape, distance between cell and pipette, cell types (nerve/heart cell), etc.

Currently, simulation only takes place in two manual steps: The first part can be controlled in the equivalent circuit and the second part is controlled manually in the Matlab simulation.

Another important point would be to perform an EIS test with the used Photocaps. This would provide better information about the electronical structure of the light-

sensitive devices. So far, the parameters could only be determined by comparison with the measured results. The main goal of the entire equivalent circuit is to incorporate the dynamic cell behavior (which was deliberately omitted initially) and though to achieve meaningful results.

Field potential measurement An idea to improve the field potential measurement would be a programmed control of a micromanipulator, which allows to approach certain positions. Especially the height of the pipette is still a problem. In order to obtain at least equal x- and y-positions, a measuring cap was developed which provides openings for the insertion of the measuring pipette, shown in 6.3. A technical drawing of this cap is shown in figure 6.2. Unfortunately, the height of the measuring pipette still causes problems and could be ensured with a self-written start-up protocol of a programmable micromanipulator.
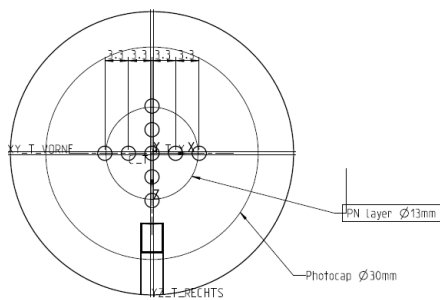

Figure 6.2.: Field potential measuring cap with predefined distances
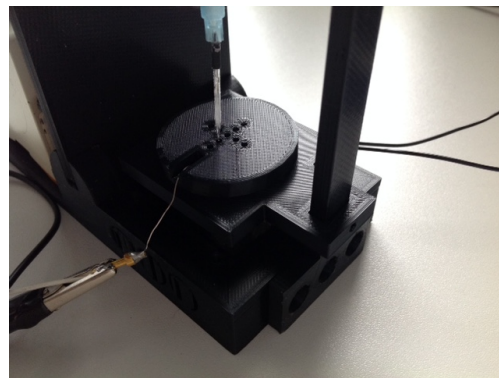

Figure 6.3.: Measurement setup of the field potential measurement setup

All in all, despite many difficulties which emerged especially in the non-reproducible measurements, reasonable and meaningful results could be achieved, which confirm the vision of the LOGOS-TBI project. I am optimistic that Photocap plans can be implemented and success will be achieved.

Appendix

The content of this appendix serves for further explanation of this Master's thesis.

A. EPR

In the following section, the results of the EPR measurement series (from 3.1 V to 10 V, with square pulse) are listed in addition to the results chapter in 4.1.2.

Figure A.1.: EPR measurement: Photovoltage curve with a Vp of 3.1 V, PULSE ON: 20 ms and PULSE OFF: 10 ms

6. Conclusion

Figure A.2.: EPR measurement: Photovoltage curve with a Vp of 4.5 V, PULSE ON: 20 ms and PULSE OFF: 10 ms

Figure A.3.: EPR measurement: Photovoltage curve with a Vp of 5 V, PULSE ON: 20 ms and PULSE OFF: 10 ms

Figure A.4.: EPR measurement: Photovoltage curve with a Vp of 6 V, PULSE ON: 20 ms and PULSE OFF: 10 ms
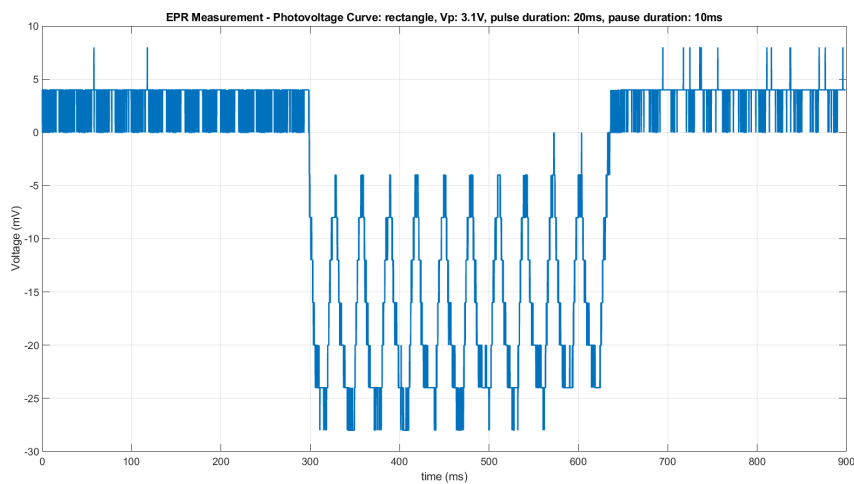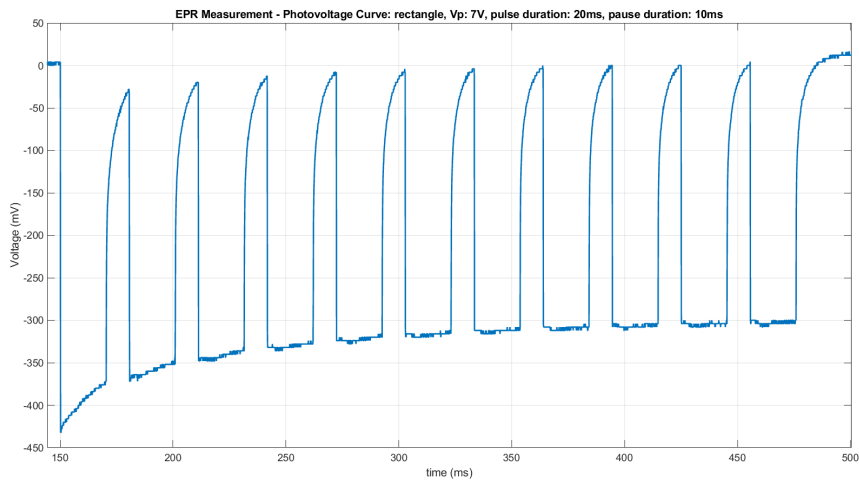

Figure A.5.: EPR measurement: Photovoltage curve with a Vp of 7 V, PULSE ON: 20 ms and PULSE OFF: 10 ms

6. Conclusion
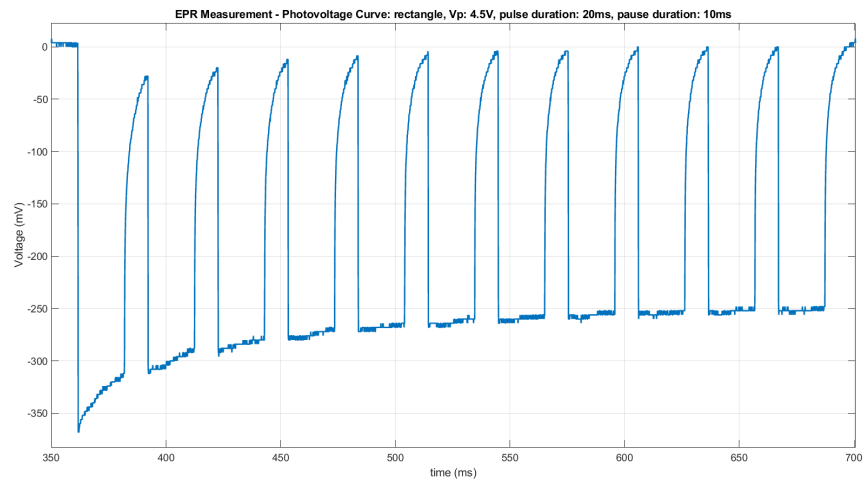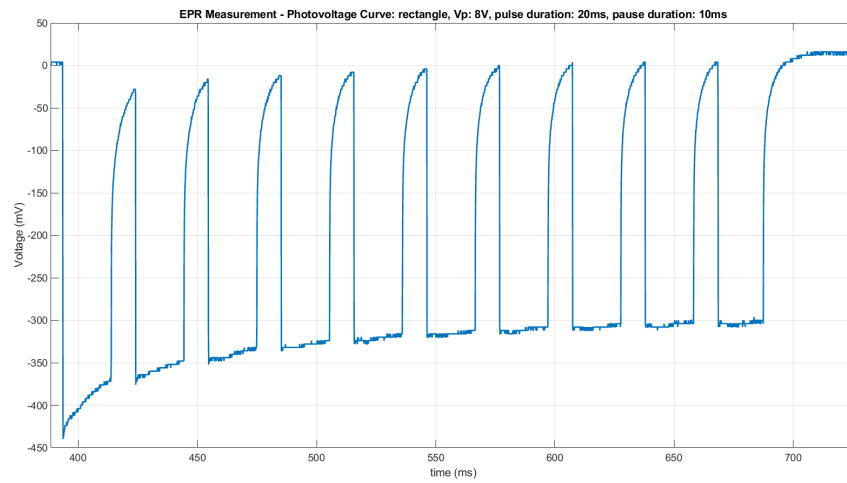

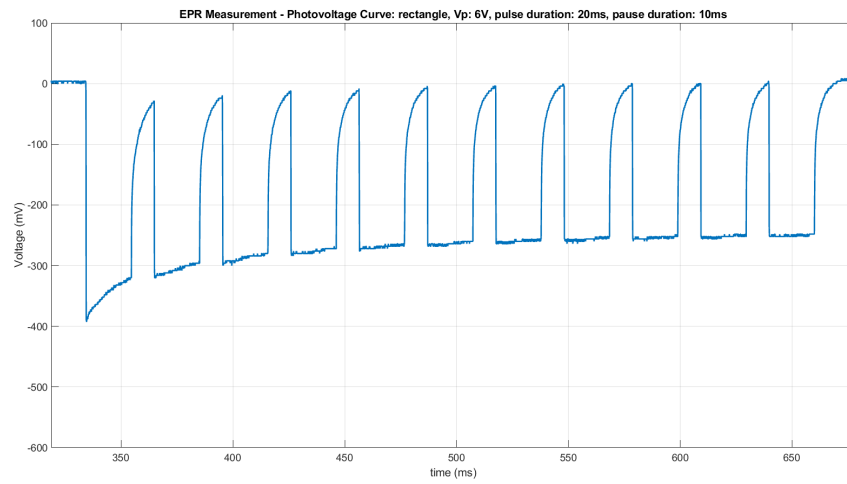Figure A.6.: EPR measurement: Photovoltage curve with a Vp of 8 V, PULSE ON: 20 ms and PULSE OFF: 10 ms
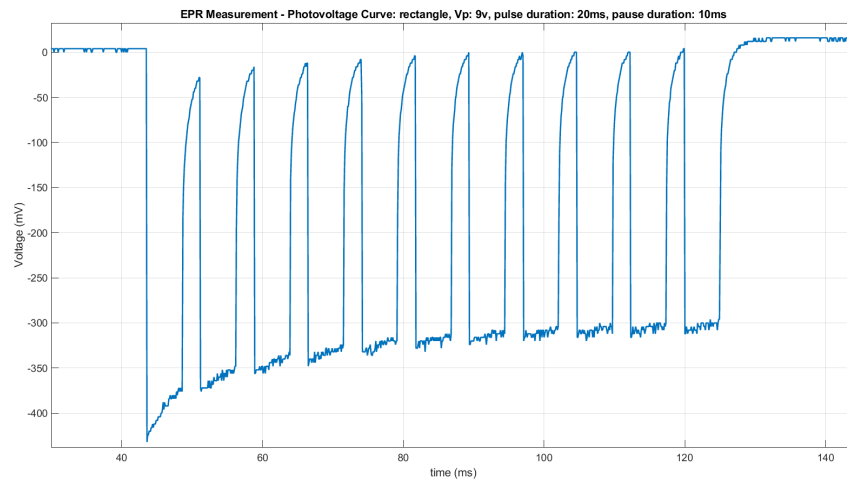
Figure A.7.: EPR measurement: Photovoltage curve with a Vp of 9 V, PULSE ON: 20 ms and PULSE OFF: 10 ms

Figure A.8.: EPR Measurement Photovoltage curve with a Vp of 10 V, PULSE ON: 20 ms
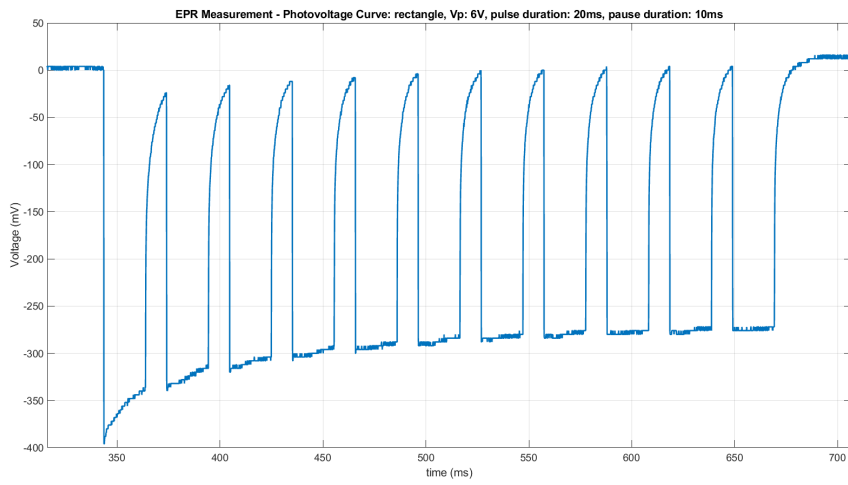and PULSE OFF: 10 ms

B. Photocap charging behavior

In the following section, the results of the charging behaviour measurement series
are listed in addition to chapter **Charging behaviour** discussed in 4.1.2.

6. Conclusion
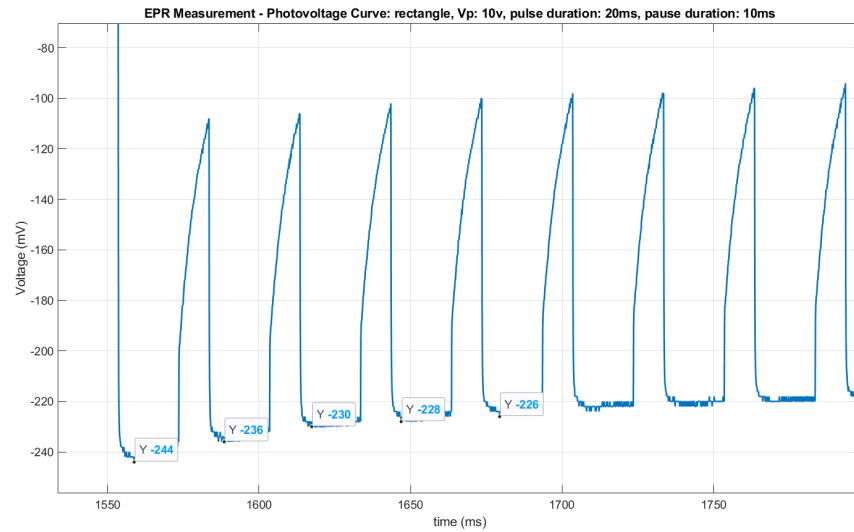
Figure B.9.: EPR Measurement curve with PULSE ON: 20 ms and PULSE OFF: 10 ms, with a $\Delta V \approx 16$ mV
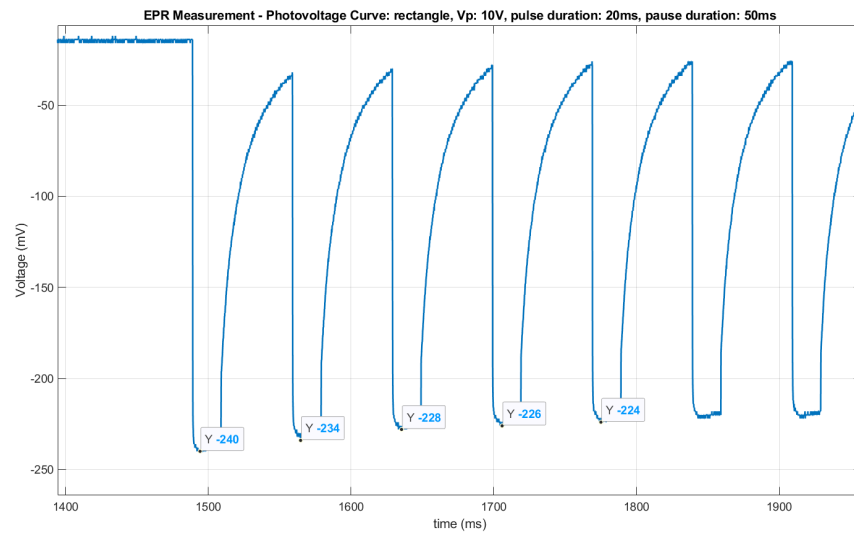
Figure B.10.: EPR Measurement curve with PULSE ON: 20 ms and PULSE OFF: 50 ms, with a $\Delta V \approx 18$ mV
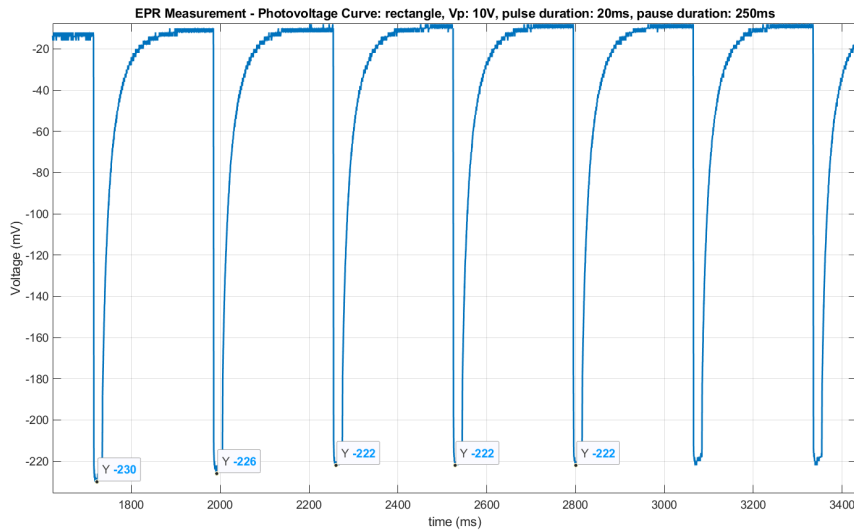
Figure B.11.: EPR Measurement curve with PULSE ON: 20 ms and PULSE OFF: 250 ms, with a $\Delta V \approx 8$ mV
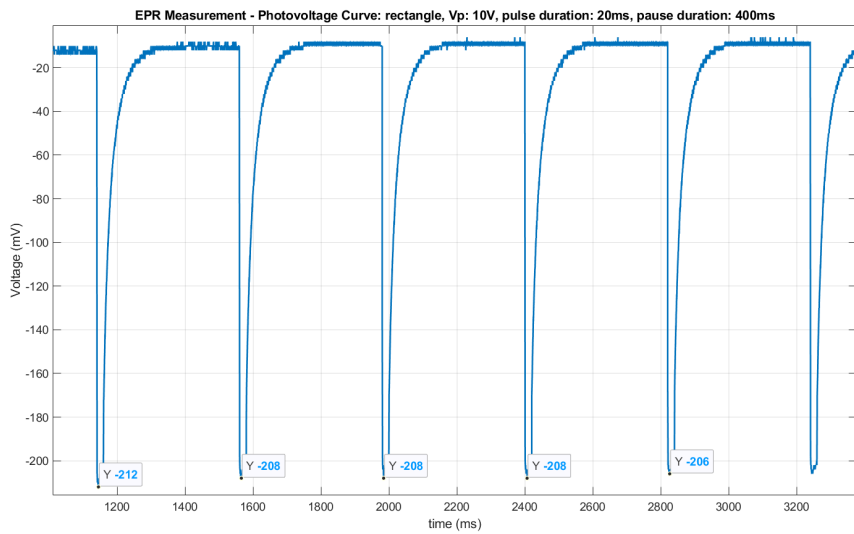
Figure B.12.: EPR Measurement curve with PULSE ON: 20 ms and PULSE OFF: 400 ms, with a $\Delta V \approx 6$ mV

C. Field potential measurements with in/ex chicken solutions

In this chapter, in addition to chapter 4.1.2, the measurement results of the distribution of the field potential with different intracellular and extracellular solutions are listed below (used in practice for chicken measurements). The first series of measurements was performed at the same x-y-z position but with different pulse lengths, shown in fig. FP Measurement with in- and extracellular chicken solutions and corresponding table C.1 with measured values.
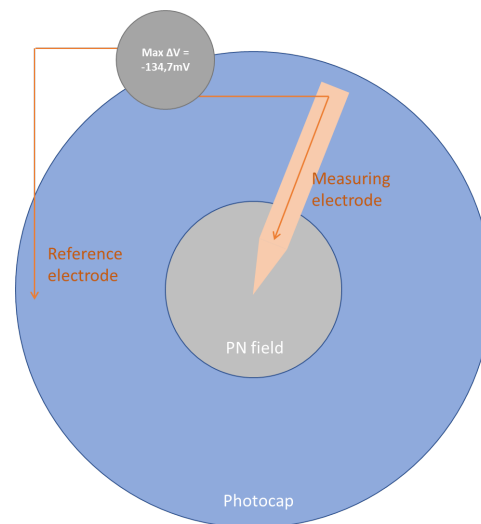
Figure C.13.: FP Measurement with in- and extracellular chicken solutions

C. Field potential measurements with in/ex chicken solutions

Table C.1.: Measuring at same x-y-z position

Reference electrode:	Hanging in the bath
Measuring electrode:	**In the center of the PN field, at approx. cell height**
Pulse(ms)	**Max measured peak (mV)**
0.25	-134.7
1	-121.3
5	-123.1
10	-125.6
100	-118.7
1000	-101.6

Another single measurement performed is shown in fig. C.14 and the corresponding table is C.2.

Figure C.14.: FP Measurement with in- and extracellular chicken solutions

Table C.2.: 10 ms pulse, 200 ms pause

Reference electrode:	Hanging in the bath on the left (outside the PN field)	
Measuring electrode:	**In the center of the PN field**	
Pulse(ms)	**Max measured peak (mV)**	**Measuring electrode height**
10	-141	>100 um above the PN field

6. Conclusion

A small measurement series was performed at the left border of the PN field at different heights, shown in fig. C.15 and the corresponding table C.3.

Figure C.15.: FP Measurement with in- and extracellular chicken solutions

Table C.3.: 10 ms pulse, 200 ms pause

| Reference electrode: | Hanging in the bath on the left (outside the PN field) | |
| Measuring electrode: | At the left border of the PN field | |
Pulse(ms)	Max measured peak (mV)	Measuring electrode height
10	-58.7	approx. 100 um above the PN field
10	-80	barely in the bath

During the measurement the pipette was moved at the same height from the right PN border to the left PN border. The movement and measured values are shown in fig. C.16 and the corresponding table C.4.

Figure C.16.: FP Measurement with in- and extracellular chicken solutions

Table C.4.: 10 ms pulse, 200 ms pause

Reference electrode:	Hanging in the bath on the left (outside the PN field)	
Measuring electrode:	At the right border of the PN field	
Pulse(ms)	Max measured peak (mV)	Measuring electrode height
10	-103.1	>100 um above the PN field

During the measurement, the measuring pipette was positioned in the middle of the PN field and then moved upwards starting at about cell height. Afterwards it was moved to the left edge of the PN field. The measurement results are shown in fig. C.17 and the corresponding table C.5.
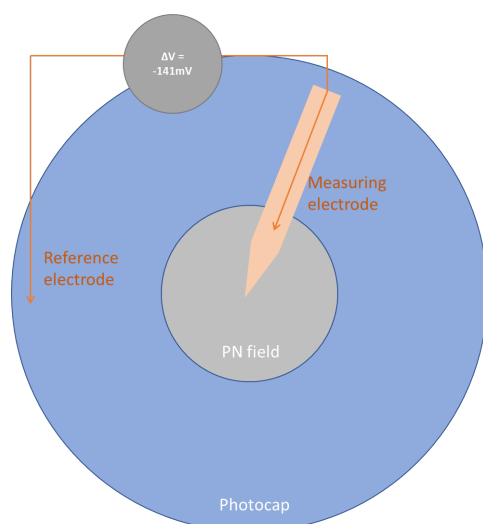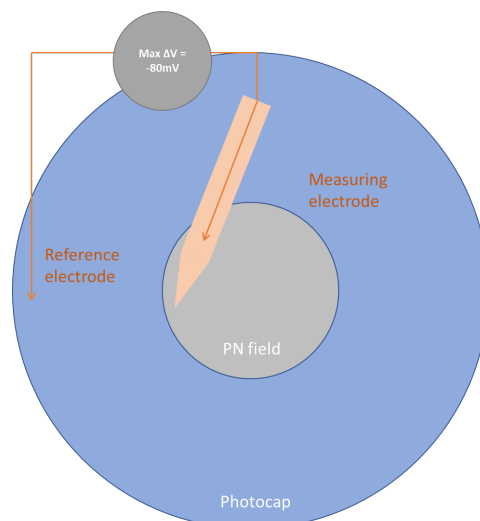
6. Conclusion
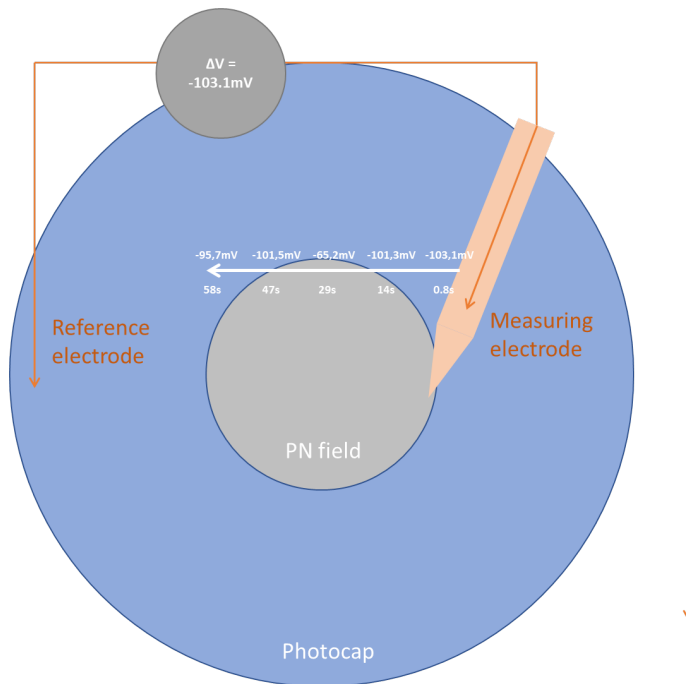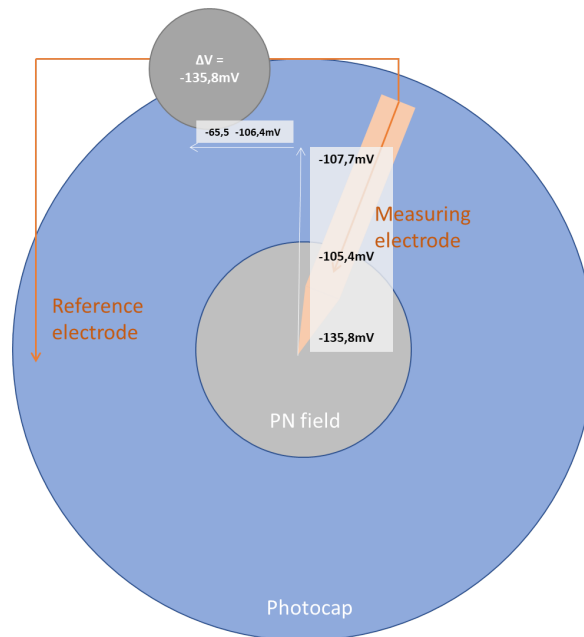

Figure C.17.: FP Measurement with in- and extracellular chicken solutions

Table C.5.: 10 ms pulse, 200 ms pause

| Reference electrode: | Hanging in the bath on the left (outside the PN field) | |
| Measuring electrode: | In the centre of the PN field | |
Pulse(ms)	Max measured peak (mV)	Measuring electrode height
10	-135.8	>100 um above the PN field

Bibliography

[1] Nos aej 33. *English: Rheobase and chronaxie are points defined along the strength-duration curve for an excitable tissue.* Oct. 2009. URL: https://commons.wikimedia.org/wiki/File:Rheobase_chronaxie.png (visited on 11/15/2019) (cit. on p. 35).

[2] G. W. Beeler and H. Reuter. "Reconstruction of the action potential of ventricular myocardial fibres." en. In: *The Journal of Physiology* 268.1 (June 1977), pp. 177–210. ISSN: 00223751. DOI: 10.1113/jphysiol.1977.sp011853. URL: http://doi.wiley.com/10.1113/jphysiol.1977.sp011853 (visited on 12/09/2019) (cit. on p. 8).

[3] *beeler_reuter_1977.png (412288).* URL: https://models.physiomeproject.org/workspace/beeler_reuter_1977/@@rawfile/45ac0567d00fa0510830d6e418cbc7d26244c9/beeler_reuter_1977.png (cit. on p. 8).

[4] L. Ebihara. "The initial inward current in spherical clusters of chick embryonic heart cells." en. In: *The Journal of General Physiology* 75.4 (Apr. 1980), pp. 437–456. ISSN: 0022-1295, 1540-7748. DOI: 10.1085/jgp.75.4.437. URL: http://www.jgp.org/cgi/doi/10.1085/jgp.75.4.437 (visited on 11/19/2019) (cit. on p. 33).

[5] L. Ebihara and E.A. Johnson. "Fast sodium current in cardiac muscle. A quantitative description." en. In: *Biophysical Journal* 32.2 (Nov. 1980), pp. 779–790. ISSN: 00063495. DOI: 10.1016/S0006-3495(80)85016-8. URL: https://linkinghub.elsevier.com/retrieve/pii/S0006349580850168 (visited on 11/05/2019) (cit. on p. 34).

[6] Präzisions Glas & Optik GmbH. *spektraler Transmissiongrad.* Nov. 2019. URL: https://www.pgo-online.com/de/kurven/pdfkurven/D/CEC020S40070011.pdf (cit. on p. 19).

[7]   *ITO-Beschichtungen | Leitfähige, transparente Schichten auf Glas.* URL:
        https://www.pgo-online.com/de/ito.html (visited on 11/14/2019)
        (cit. on p. 19).

[8]   Marie Jakešová et al. "Optoelectronic control of single cells using
        organic photocapacitors." en. In: *Science Advances* 5.4 (Apr. 2019),
        eaav5265. ISSN: 2375-2548. DOI: 10.1126/sciadv.aav5265. URL: http:
        //advances.sciencemag.org/lookup/doi/10.1126/sciadv.aav5265
        (visited on 11/12/2019) (cit. on pp. 15, 16, 18, 21, 22, 24, 60, 61).

[9]   Marie Jakešová et al. "Optoelectronic control of single cells using
        organic photocapacitors." en. In: *Science Advances* 5.4 (Apr. 2019),
        eaav5265. ISSN: 2375-2548. DOI: 10.1126/sciadv.aav5265. URL: http:
        //advances.sciencemag.org/lookup/doi/10.1126/sciadv.aav5265
        (visited on 11/06/2019) (cit. on pp. 16, 46).

[10]   Dennis L. Kasper et al., eds. *Harrisons Innere Medizin. Reg: Register.* de.
        19. Auflage. OCLC: 964693673. New York, NY: McGraw-Hill Educa-
        tion, 2016. ISBN: 978-3-940615-50-3 (cit. on p. 3).

[11]   W. Krassowska and J.C. Neu. "Response of a single cell to an external
        electric field." en. In: *Biophysical Journal* 66.6 (June 1994), pp. 1768–1776.
        ISSN: 00063495. DOI: 10.1016/S0006-3495(94)80971-3. URL: https:
        //linkinghub.elsevier.com/retrieve/pii/S0006349594809713
        (visited on 11/19/2019) (cit. on p. 16).

[12]   Dongchul C. Lee and Warren M. Grill. "Polarization of a Spherical
        Cell in a Nonuniform Extracellular Electric Field." en. In: *Annals of
        Biomedical Engineering* 33.5 (May 2005), pp. 603–615. ISSN: 0090-6964,
        1573-9686. DOI: 10.1007/s10439-005-2397-3. URL: http://link.
        springer.com/10.1007/s10439-005-2397-3 (visited on 11/12/2019)
        (cit. on p. 17).

[13]   C H Luo and Y Rudy. "A model of the ventricular cardiac action
        potential. Depolarization, repolarization, and their interaction." en.
        In: *Circulation Research* 68.6 (June 1991), pp. 1501–1526. ISSN: 0009-
        7330, 1524-4571. DOI: 10.1161/01.RES.68.6.1501. URL: https:
        //www.ahajournals.org/doi/10.1161/01.RES.68.6.1501 (visited
        on 11/06/2019) (cit. on pp. 8, 10, 34).

[14] *luo_rudy_i_1991.png (395281)*. URL: https://models.cellml.org/workspace/luo_rudy_1991/@@rawfile/88c466ea509fa9d83741b89def0bdb4208c3fde7/luo_rudy_i_1991.png (cit. on p. 9).

[15] Anna Maier. *Funktionelle Koordinationspolymerfilme aus Polyiminoarylenen mit Terpyridin-Liganden*. de. Google-Books-ID: 2n3gDiO3NikC. disserta Verlag, 2011. ISBN: 978-3-942109-48-2 (cit. on p. 39).

[16] P. Marszalek, D.S. Liu, and T.Y. Tsong. "Schwan equation and transmembrane potential induced by alternating electric field." en. In: *Biophysical Journal* 58.4 (Oct. 1990), pp. 1053–1058. ISSN: 00063495. DOI: 10.1016/S0006-3495(90)82447-4. URL: https://linkinghub.elsevier.com/retrieve/pii/S0006349590824474 (visited on 12/09/2019) (cit. on p. 17).

[17] *MePTCDI*. de. Page Version ID: 194172920. Nov. 2019. URL: https://de.wikipedia.org/w/index.php?title=MePTCDI&oldid=194172920 (visited on 12/09/2019) (cit. on p. 19).

[18] Daniel R. Merrill, Marom Bikson, and John G.R. Jefferys. "Electrical stimulation of excitable tissue: design of efficacious and safe protocols." en. In: *Journal of Neuroscience Methods* 141.2 (Feb. 2005), pp. 171–198. ISSN: 01650270. DOI: 10.1016/j.jneumeth.2004.10.020. URL: https://linkinghub.elsevier.com/retrieve/pii/S0165027004003826 (visited on 11/06/2019) (cit. on pp. 14, 16, 20).

[19] Narendran Sekar Ramaraja P Ramasamy. "Electrochemical Impedance Spectroscopy for Microbial Fuel Cell Characterization." en. In: *Journal of Microbial & Biochemical Technology* (2013). ISSN: 19485948. DOI: 10.4172/1948-5948.S6-004. URL: https://www.omicsonline.org/electrochemical-impedance-spectroscopy-for-microbial-fuel-cell-characterization-1948-5948.S6-004.php?aid=18518 (visited on 12/09/2019) (cit. on p. 28).

[20] David Rand et al. "Direct Electrical Neurostimulation with Organic Pigment Photocapacitors." en. In: *Advanced Materials* 30.25 (June 2018), p. 1707292. ISSN: 0935-9648, 1521-4095. DOI: 10.1002/adma.201707292. URL: https://onlinelibrary.wiley.com/doi/abs/10.1002/adma.201707292 (visited on 11/06/2019) (cit. on pp. 14, 48, 49, 51, 61).

Bibliography

[21]   David Rand et al. "Direct Electrical Neurostimulation with Organic Pigment Photocapacitors." en. In: *Advanced Materials* 30.25 (June 2018), p. 1707292. ISSN: 0935-9648, 1521-4095. DOI: 10.1002/adma.201707292. URL: https://onlinelibrary.wiley.com/doi/abs/10.1002/adma.201707292 (visited on 11/06/2019) (cit. on pp. 28, 29, 46, 48, 63).

[22]   J.Patrick Reilly. *Electrical Stimulation and Electropathology*. 1992. ISBN: 0-521-41791-0 (cit. on pp. 1, 6).

[23]   Jürgen Rettinger, Silvia Schwarz, and Wolfgang Schwarz. *Elektrophysiologie: Grundlagen - Methoden - Anwendungen*. de. Lehrbuch. OCLC: 1048742447. Berlin, Germany: Springer Spektrum, 2018. ISBN: 978-3-662-56661-9 978-3-662-56662-6 (cit. on p. 1).

[24]   Ingmar Schoen and Peter Fromherz. "The Mechanism of Extracellular Stimulation of Nerve Cells on an Electrolyte-Oxide-Semiconductor Capacitor." en. In: *Biophysical Journal* 92.3 (Feb. 2007), pp. 1096–1111. ISSN: 00063495. DOI: 10.1529/biophysj.106.094763. URL: https://linkinghub.elsevier.com/retrieve/pii/S0006349507709177 (visited on 11/06/2019) (cit. on pp. 14, 29, 30, 48, 51).

[25]   Michał Sobaszek et al. "Enhancing electrochemical properties of an ITO-coated lossy-mode resonance optical fiber sensor by electrodeposition of PEDOT:PSS." en. In: *Optical Materials Express* 9.7 (July 2019), p. 3069. ISSN: 2159-3930. DOI: 10.1364/OME.9.003069. URL: https://www.osapublishing.org/abstract.cfm?URI=ome-9-7-3069 (visited on 11/15/2019) (cit. on pp. 19, 49).

[26]   Bradley A. Stone, Melvyn Lieberman, and Wanda Krassowska. "Field Stimulation of Isolated Chick Heart Cells.: Comparison of Experimental and Theoretical Activation Thresholds." en. In: *Journal of Cardiovascular Electrophysiology* 10.1 (Jan. 1999), pp. 92–107. ISSN: 1045-3873, 1540-8167. DOI: 10.1111/j.1540-8167.1999.tb00646.x. URL: http://doi.wiley.com/10.1111/j.1540-8167.1999.tb00646.x (visited on 11/15/2019) (cit. on pp. 33, 64).

[27]   Bahman Tahayori and Socrates Dokos. "Optimal stimulus profiles for neuroprosthetic devices: Monophasic versus biphasic stimulation." en. In: *2013 35th Annual International Conference of the IEEE Engineering in Medicine and Biology Society (EMBC)*. Osaka: IEEE, July 2013, pp. 5978–5981. ISBN: 978-1-4577-0216-7. DOI: 10.1109/EMBC.2013.6610914.

URL: http://ieeexplore.ieee.org/document/6610914/ (visited on 11/12/2019) (cit. on p. 14).

[28] converted to SVG by Original by en:User:Chris 73 tiZom updated by en:User:Diberri. *English: Schematic of an action potential*. URL: https://commons.wikimedia.org/wiki/File:Action_potential.svg (visited on 11/15/2019) (cit. on p. 3).

[29] L. Tung and J.R. Borderies. "Analysis of electric field stimulation of single cardiac muscle cells." en. In: *Biophysical Journal* 63.2 (Aug. 1992), pp. 371–386. ISSN: 00063495. DOI: 10.1016/S0006-3495(92)81632-6. URL: https://linkinghub.elsevier.com/retrieve/pii/S0006349592816326 (visited on 11/06/2019) (cit. on pp. 13, 16).

[30] Aristizabal Botero William, H Salas Alvaro, and Janeth Gonzalez Colorado Silvia. "The Hodgkin-Huxley neuron model on the fast phase plane." en. In: *International Journal of Physical Sciences* 8.20 (May 2013), pp. 1049–1057. ISSN: 1992-1950. DOI: 10.5897/IJPS11.1334. URL: http://academicjournals.org/journal/IJPS/article-abstract/7C3E6C130021 (visited on 11/19/2019) (cit. on p. 59).

[31] X Zhou et al. "Effects of monophasic and biphasic shocks on action potentials during ventricular fibrillation in dogs." en. In: *Circulation Research* 73.2 (Aug. 1993), pp. 325–334. ISSN: 0009-7330, 1524-4571. DOI: 10.1161/01.RES.73.2.325. URL: https://www.ahajournals.org/doi/10.1161/01.RES.73.2.325 (visited on 11/12/2019) (cit. on p. 15).